OPEN ACCESS

Original research

FSTL1 promotes liver fibrosis by reprogramming macrophage function through modulating the intracellular function of PKM2

Jianhua Rao ,[1,2,3] Hao Wang,[1,2] Ming Ni,[1,2] Zeng Wang,[1,2] Ziyi Wang,[1,2] Song Wei,[1,2] Mu Liu,[1,2] Peng Wang,[1,2] Jiannan Qiu,[1,2] Lei Zhang,[1,2] Chen Wu,[1,2] Hongbing Shen,[2,4] Xuehao Wang ,[1,2] Feng Cheng,[1,2,3] Ling Lu [1,2,3,4]

► Additional supplemental material is published online only. To view, please visit the journal online (http://dx.doi.org/10.1136/gutjnl-2021-325150).

For numbered affiliations see end of article.

Correspondence to
Dr Ling Lu, Dr Feng Cheng and Dr Jianhua Rao, Hepatobiliary Center of The First Affiliated Hospital, Nanjing Medical University, Nanjing, China; lvling@njmu.edu.cn, docchengfeng@njmu.edu.cn, raojh@njmu.edu.cn

Received 14 May 2021
Accepted 23 January 2022
Published Online First 9 February 2022

To cite: Rao J, Wang H, Ni M, *et al*. *Gut* 2022;**71**:2539–2550.

ABSTRACT

Objective Follistatin-like protein 1 (FSTL1) is widely recognised as a secreted glycoprotein, but its role in modulating macrophage-related inflammation during liver fibrosis has not been documented. Herein, we aimed to characterise the roles of macrophage FSTL1 in the development of liver fibrosis.

Design Expression analysis was conducted with human liver samples obtained from 33 patients with liver fibrosis and 18 individuals without fibrosis serving as controls. Myeloid-specific FSTL1-knockout ($FSTL1^{M\text{-}KO}$) mice were constructed to explore the function and mechanism of macrophage FSTL1 in 3 murine models of liver fibrosis induced by carbon tetrachloride injection, bile duct ligation or a methionine-deficient and choline-deficient diet.

Results FSTL1 expression was significantly elevated in macrophages from fibrotic livers of both humans and mice. Myeloid-specific FSTL1 deficiency effectively attenuated the progression of liver fibrosis. In $FSTL1^{M\text{-}KO}$ mice, the microenvironment that developed during liver fibrosis showed relatively less inflammation, as demonstrated by attenuated infiltration of monocytes/macrophages and neutrophils and decreased expression of proinflammatory factors. $FSTL1^{M\text{-}KO}$ macrophages exhibited suppressed proinflammatory M1 polarisation and nuclear factor kappa B pathway activation in vivo and in vitro. Furthermore, this study showed that, through its FK domain, FSTL1 bound directly to the pyruvate kinase M2 (PKM2). Interestingly, FSTL1 promoted PKM2 phosphorylation and nuclear translocation, reduced PKM2 ubiquitination to enhance PKM2-dependent glycolysis and increased M1 polarisation. Pharmacological activation of PKM2 (DASA-58) partially countered FSTL1-mediated glycolysis and inflammation.

Conclusion Macrophage FSTL1 promotes the progression of liver fibrosis by inducing M1 polarisation and inflammation based on the intracellular PKM2 reprogramming function of macrophages.

Significance of this study

What is already known on this subject?

⇒ Macrophage has been identified as key regulators of the liver inflammation, which is critical for the progression or resolution of liver fibrosis.

⇒ Follistatin-like protein 1 (FSTL1) is widely regarded as a secreted glycoprotein with regulatory functions in many diseases.

⇒ Secreted/Circulatory FSTL1 has been proposed as a promoting protein in inflammation or fibrosis-related diseases in a secretion-dependent manner.

What are the new findings?

⇒ FSTL1 expression in macrophages is increased and is positively correlated with histological stages of liver fibrosis in humans and mice.

⇒ Myeloid FSTL1 deficiency suppresses M1 polarisation, reduces proinflammatory mediator expression and macrophage/neutrophil recruitment and alleviates liver fibrosis.

⇒ FSTL1 directly binds to pyruvate kinase M2 (PKM2), inhibits ubiquitin-mediated degradation, enhances the stability of cytoplasmic PKM2 and promotes PKM2 phosphorylation and nuclear translocation in macrophages.

⇒ PKM2 is critical for FSTL1-mediated M1 polarisation, inflammation and glycolysis in macrophages.

How might it impact on clinical practice in the foreseeable future?

⇒ Our findings provide a rationale for novel therapeutic strategies to ameliorate macrophage-mediated liver inflammation and fibrosis.

INTRODUCTION

Liver fibrosis is the most common consequence of chronic liver diseases, and it causes >1 million deaths worldwide every year.[1] Advanced liver fibrosis, especially its end-stage form, cirrhosis, is generally regarded as an incurable disease, and liver transplantation is the sole and definitive treatment option.[2] Various aetiologies, such as viral hepatitis, alcohol abuse, cholestasis or, as recently discovered, non-alcoholic steatohepatitis (NASH), can cause chronic liver injury and subsequent liver fibrosis.[3] However, this mechanism of precise regulation is

problematic and uncontrollable, especially when liver injury persists. Currently, liver fibrosis is widely recognised as a dynamic cascade fuelled by persistent and excessive activation of hepatic inflammation that develops in response to repetitive or chronic hepatocyte injury irrespective of aetiology.[4 5] Uncontrolled chronic inflammation is a non-negligible driving force transforming self-limited tissue repair processes into a vicious cycle that boosts the progression of liver fibrosis.[6]

Immune cells, especially liver-residing Kupffer cells and recruited macrophages, have been identified as key regulators of the liver inflammation that are key to the progression or resolution of liver fibrosis.[7] Damaged hepatocytes release danger-associated molecular patterns (DAMPs) to activate Kupffer cells and infiltrated macrophages. Activated macrophages release various cytokines, causing direct damage to liver parenchymal cells, enhancing inflammatory cell infiltration and activating hepatic stellate cells (HSCs).[8 9] Hepatic macrophages have reportedly promoted liver fibrosis by increasing the survival of activated HSCs in an nuclear factor kappa B (NF-κB)-dependent manner.[10] In addition, macrophage-derived transforming growth factor (TGF)-β has been recognised as a key molecule initiating HSC activation.[11] Furthermore, several studies have indicated that toll-like receptor (TLR)-4 and TLR-9 signalling pathways mediate crosstalk between inflammatory and fibrotic factors.[12 13] Thus, a deeper understanding of the underlying mechanisms involved in macrophage-orchestrated chronic liver inflammation can provide valuable information that may help to halt and effectively reverse ongoing liver fibrosis.

Follistatin-like protein 1 (FSTL1) is widely known as a secreted glycoprotein with regulatory functions in many diseases and is indispensable during embryogenesis.[14] FSTL1-deficient mice suffer from postnatal death as a result of respiratory failure, while hypomorphic mice develop spontaneous emphysema.[15 16] In addition to its regulatory functions seen in embryonic development, the role of FSTL1 in inflammation has been widely studied in the past decade.[17 18] However, whether FSTL1 plays a proinflammatory role is still debated.[17–21] FSTL1 is widely regarded as a fibrosis-promoting protein both outside and inside the liver, but previous studies have mainly focused on the profibrotic functions of FSTL1 in mesenchymal cells such as fibroblasts, not in inflammatory cells such as macrophages.[22–24] Pyruvate kinase M2 (PKM2) is directly involved in the metabolic reprogramming (aerobic glycolysis) associated with cancer and the inflammatory response.[25 26] Importantly, PKM2 has been shown to control macrophage metabolic remodelling in inflammation. PKM2 interacts with hypoxia-inducible factor 1α (HIF-1α) and activates the HIF-1α-dependent transcription of enzymes necessary for aerobic glycolysis in macrophages.[26]

Herein, we aimed to characterise the roles and mechanisms of macrophage FSTL1 during liver fibrosis. First, macrophage FSTL1 expression was assessed in patients and mice with liver fibrosis/cirrhosis. Second, we created a myeloid-specific FSTL1-knockout ($FSTL1^{M\text{-}KO}$) mouse to study the function of macrophage FSTL1 in different mouse models of liver fibrosis. Third, the functional effects and underlying mechanisms of FSTL1 on macrophage-related inflammation were thoroughly analysed in vivo and in vitro.

MATERIALS AND METHODS

Human liver samples

Liver samples were obtained from patients who underwent hepatectomy or percutaneous liver biopsy. Liver samples were collected from 18 patients with benign liver diseases (postoperative pathological diagnosis showed hemangioma with no liver fibrosis or obvious steatosis; 18 liquid nitrogen-frozen samples and 6 paraffin-embedded samples) and 33 patients with pathologically diagnosed liver fibrosis (33 liquid nitrogen-frozen samples and 16 paraffin-embedded slides). The control individuals that were included had no history of diabetes, alcohol abuse or viral hepatitis. Control samples were taken from normal liver tissues at the edge of resected hemangioma. Pathological diagnosis of liver fibrosis was determined by senior pathologists based on H&E and Masson's staining. Samples from patients with liver fibrosis were graded according to the fibrosis scoring systems by two senior pathologists (online supplemental tables 1–4).

Animal experiments

All mice were housed in an SPF level animal facility with controlled temperature and humidity on a 12–12 hour light-dark cycle with food and water supplied ad libitum. For the carbon tetrachloride (CCl_4) injection-induced liver fibrosis, male mice aged 6–8 weeks were randomly assigned to receive intraperitoneal injection of olive oil or CCl_4 (10% v/v dissolved in olive oil, 2 mL/kg) twice per week for 8 weeks. For bile duct ligation (BDL)-induced liver fibrosis, male mice aged 6–8 weeks were subjected to surgical intervention. Briefly, mice were anaesthetised by isoflurane inhalation. After skin disinfection, a midline abdominal incision was made. The common bile ducts were exposed and ligated using 5–0 non-absorbable sutures. Samples were collected 4 weeks after surgery. To induce liver fibrosis by methionine-deficient and choline-deficient (MCD) diet, male mice aged 8–10 weeks were fed a normal chow (NC) or MCD diet (A02082002BR, Research Diets) for an indicated duration of up to 8 weeks.

Statistical analysis

Unpaired Student's t-test or Mann-Whitney U test were performed in group comparisons by using GraphPad Prism (V.8.0, GraphPad Software). P values <0.05 were considered to be statistically significant.

For detailed methods and materials, please refer to online supplemental materials.

RESULTS

FSTL1 expression is increased in macrophages in fibrotic liver tissues

First, we aimed to characterise FSTL1 expression among fibrotic liver samples. We collected 51 human liver samples including normal and fibrosis liver tissues (online supplemental tables 1–4). As indicated by H&E staining, Masson's staining and messenger RNA (mRNA) expression of tissue inhibitor of metalloproteinase 1 (TIMP-1) and collagen 1A1 (COL1A1), our liver samples showed different histological stages of fibrosis with fair between-group comparability (online supplemental figure 1A,B). Interestingly, the mRNA and protein expression of FSTL1 was markedly elevated in fibrotic livers compared with normal control livers (figure 1A,B). Next, we determined whether FSTL1 expression was mainly elevated in liver macrophages. Dual immunofluorescence staining showed that FSTL1 was primarily expressed on macrophages in human fibrotic livers (figure 1C and online supplemental figure 1C). Then, we used publicly available omics data on patient samples to validate these results. Virus-mediated and NASH-induced liver fibrosis are common pathological processes in liver fibrosis worldwide. By reanalysing a published dataset, we found that FSTL1 expression

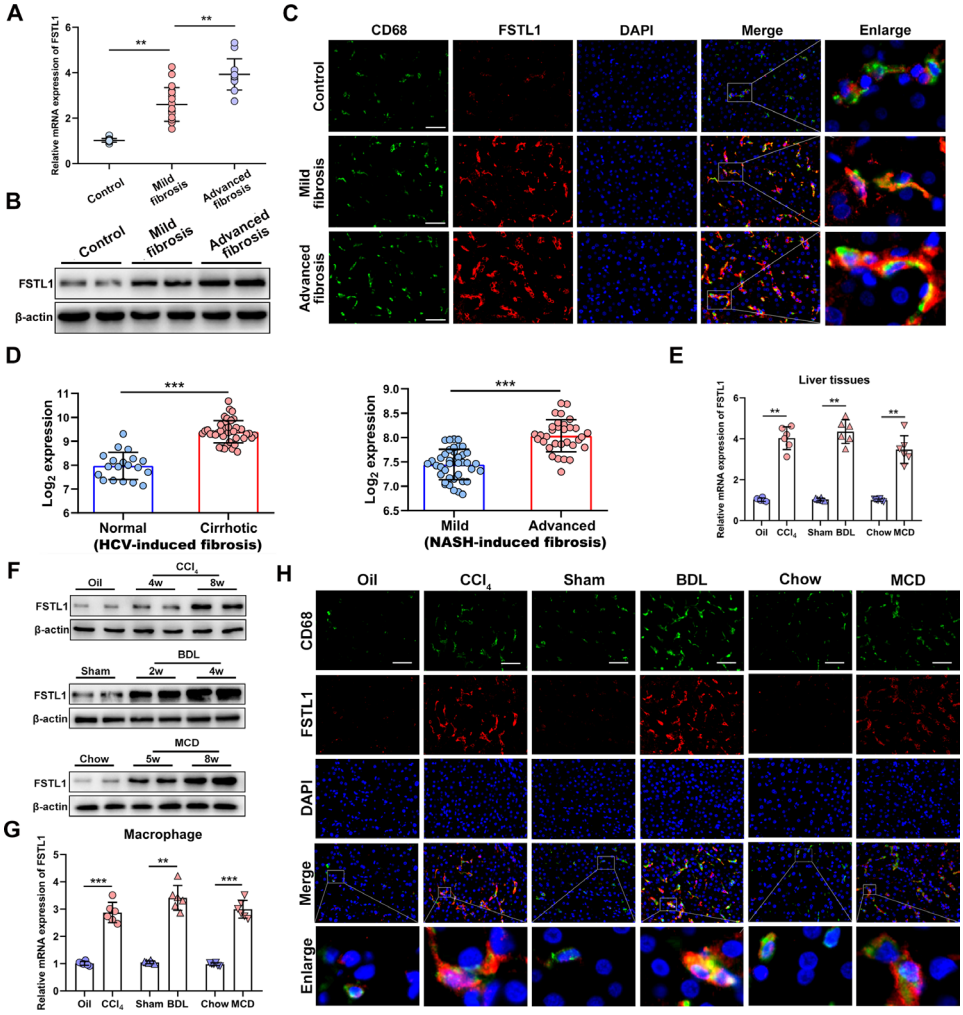

Figure 1 Follistatin-like protein 1 (FSTL1) expression is increased in macrophage of liver fibrosis tissues. Human dada (A–D) and mice data (E–H): (A) FSTL1 messenger RNA (mRNA) expression and (B) protein expression in human liver samples; (C) dual-immunofluorescence staining of FSTL1 and CD68 in liver samples; (D) liver FSTL1 expression among patients with HCV or non-alcoholic steatohepatitis (NASH)-induced liver fibrosis as determined by microarray data; (E) FSTL1 mRNA expression and (F) protein expression in murine livers; (G) FSTL1 mRNA expression in isolated mice liver macrophages; (H) dual-immunofluorescence staining of FSTL1 and CD68 in murine livers. Human samples: control (n=18), mild fibrosis (n=20), advanced fibrosis (n=13); mice samples (n=6–8 per group). Data were presented as mean±SEM; scale bars, 50 µm; **p<0.01, ***p<0.001. BDL, bile duct ligation; CCl_4, carbon tetrachloride; MCD, methionine-deficient and choline-deficient diet.

was significantly elevated in HCV-induced or NASH-induced liver fibrosis (figure 1D).[27 28]

To confirm these findings, we explored FSTL1 expression in three widely recognised animal models of liver fibrosis, namely, CCl_4 injection-induced, BDL-induced and the MCD diet-induced fibrosis. FSTL1 expression was significantly increased in liver tissues obtained from all models (figure 1E,F). These results were validated using three publicly available omics datasets (online supplemental figure 1D).[29–31] Then, we isolated liver macrophages from fibrotic livers of mice. Consistently, FSTL1 mRNA expression levels were significantly increased in macrophages isolated from fibrotic livers (figure 1G). Dual-immunofluorescence staining furthermore showed $FSTL1^+CD68^+$ macrophages were significantly more in fibrotic livers than control livers (figure 1H). In addition, we revealed FSTL1 was higher expression on macrophages, lower expression on HSCs and non-expression on hepatocytes in liver fibrosis tissues (online supplemental figure 2A,B). Taken together, these findings demonstrate that FSTL1 expression is significantly increased in liver tissues, especially in macrophages of fibrotic livers.

Myeloid FSTL1 deficiency alleviates liver fibrosis

To test the function of $FSTL1^+$ macrophages in liver fibrosis, we used the Cre-LoxP system to create myeloid-specific FSTL1-deficient ($FSTL1^{M\text{-}KO}$) mice. Then, liver fibrosis was induced in $FSTL1^{FL/FL}$ and $FSTL1^{M\text{-}KO}$ mice with CCl_4 injection, BDL or a MCD diet. Figure 2A shows that liver fibrosis was markedly lower in the $FSTL1^{M\text{-}KO}$ mice than in the $FSTL1^{FL/FL}$ mice, as revealed by Masson's, Sirius Red and alfa-smooth muscle actin (α-SMA) staining. In addition, lower serum alanine aminotransferase and aspartate aminotransferase levels postchallenge were detected in $FSTL1^{M\text{-}KO}$ mice (figure 2B). Moreover, expressions of TGF-β, TIMP-1 and collagen I were markedly lower in liver tissues from the $FSTL^{M\text{-}KO}$ mice than that in their littermate controls (figure 2C). Western blot (WB) analysis further showed FSTL1 deficiency reduced the expression of collagen I, α-SMA and TIMP-1 in fibrotic liver tissues compared with that in the

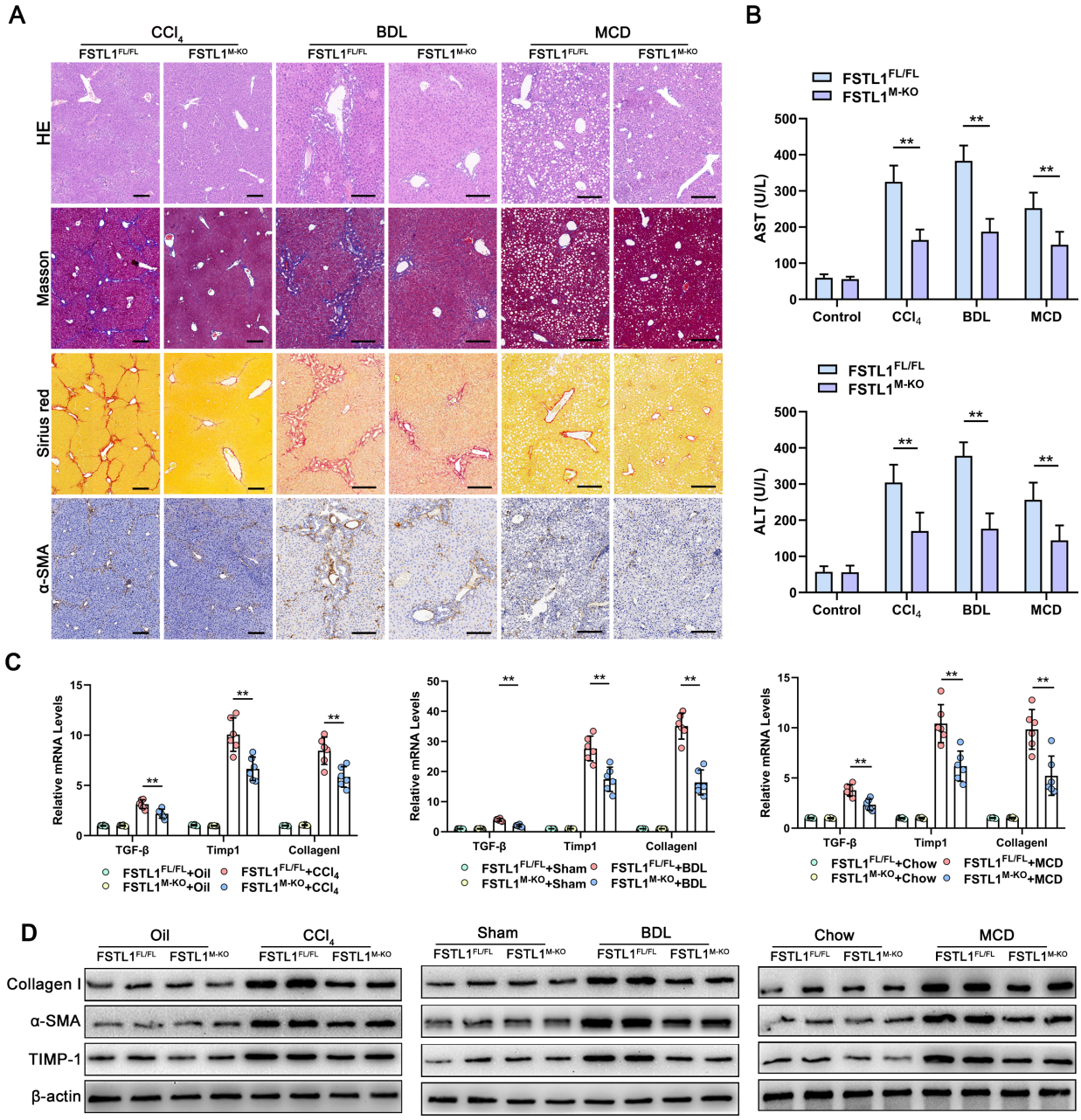

Figure 2 Myeloid follistatin-like protein 1 (FSTL1) deficiency alleviates mice liver fibrosis. (A) The degree of fibrosis was evaluated by H&E, Masson's, Sirius Red and alfa-smooth muscle actin (α-SMA) immunobiological staining; (B) serum alanine aminotransferase (ALT) and aspartate aminotransferase (AST) was measured. (C) Messenger RNA (mRNA) expression of transforming growth factor (TGF)-β, tissue inhibitor of metalloproteinase 1 (TIMP-1) and collagen I was quantified by quantitative reverse transcription-PCR and (D) protein expression of collagen I, α-SMA and TIMP-1 was analysed by western blot (WB) analysis in liver samples. Data were presented as mean±SEM; n=6–8 per group; scale bars, 50 µm; **p<0.01. BDL, bile duct ligation; CCl_4, carbon tetrachloride; MCD, methionine-deficient and choline-deficient diet.

control tissues (figure 2D). Our results suggest that myeloid FSTL1 deficiency attenuates hepatic fibrosis in mice.

Myeloid FSTL1 deficiency attenuates inflammation and macrophage/neutrophil recruitment in fibrotic livers

Next, we examined the impact of $FSTL1^{+}$ macrophages on local inflammation in fibrotic liver tissues. Figure 3A shows lower expression of tumour necrosis factor (TNF)-α and interleukin (IL)-1β, and higher expression of IL-10 in fibrotic livers obtained from $FSTL1^{M\text{-}KO}$ mice than controls. Consistently, serum levels of TNF-α and IL-1β were lower, while IL-10 was higher in $FSTL1^{M\text{-}KO}$ mice than their littermates (figure 3B). Furthermore, we evaluated the accumulation of hepatic inflammatory cells by F4/80 and CD11b (macrophage markers) and Ly6G (a neutrophil marker) staining in fibrotic liver tissues. Compared with the $FSTL1^{FL/FL}$ mouse, myeloid-specific FSTL1 deficiency markedly decreased macrophage and neutrophil infiltration in fibrotic liver tissues (figure 3C–E).

Myeloid FSTL1 deficiency suppresses M1 polarisation and NF-κB pathway activation in fibrotic livers

As mentioned above, myeloid-specific FSTL1 deficiency alleviated liver inflammation, suggesting that FSTL1 may promote M1 polarisation. First, we analysed the quantification of M1

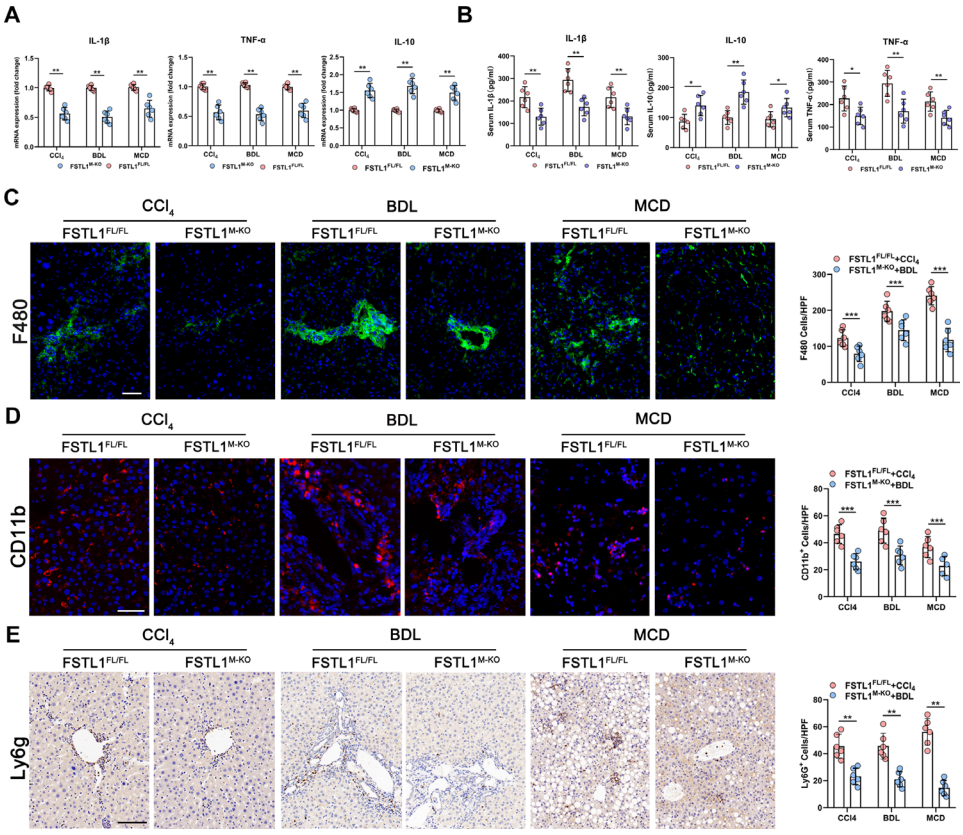

Figure 3 Myeloid follistatin-like protein 1 (FSTL1) deficiency attenuates inflammation in mice fibrotic livers. (A) Messenger RNA (mRNA) expression of tumour necrosis factor (TNF)-α, interleukin (IL)-1β and IL-10 was quantified in liver tissues; (B) serum TNF-α, IL-1β and IL-10 were measured by ELISA. (C) F4/80, (D) CD11b and (E) Ly6G were detected by immunofluorescence, and quantified as numbers of positive cells per high power field (HPF). Data were presented as mean±SEM; n=6–8 per group; scale bars, 50 µm; *p<0.05, **p<0.01, ***p<0.001. BDL, bile duct ligation; CCl_4, carbon tetrachloride; MCD, methionine-deficient and choline-deficient diet.

macrophages in liver slices, and the results showed that fewer $iNOS^+CD68^+$ macrophages were observed in the $FSTL1^{M\text{-}KO}$ mice than in the $FSTL1^{FL/FL}$ mice (figure 4A). In addition, in the $FSTL1^{M\text{-}KO}$ mice, the mRNA expression of inducible nitric oxide synthase (iNOS) was downregulated but Arg1 was upregulated in the fibrotic livers (figure 4B). WB analysis showed that myeloid FSTL1-deficient mice exhibited decreased expression of iNOS and p-STAT1 and increased expression of p-STAT6 in fibrotic livers compared with the control livers (figure 4C). The TLR-4/NF-κB pathway is a well-characterised regulatory pathway intensively involved in macrophage-orchestrated acute/chronic liver inflammation.[10] Herein, immunostaining and WB analysis of fibrotic livers also revealed that $FSTL1^{M\text{-}KO}$ mice exhibited depressed TLR-4/NF-κB pathway activation (figure 4D,E).

FSTL1 directly binds with PKM2 and enhances the stability of PKM2 in macrophages

To further investigate the mechanism underlying the regulatory role of macrophage FSTL1 during liver fibrosis, immunoprecipitation (IP) assays and LC-MS/MS screening were performed to explore FSTL1 binding to potential proteins in macrophages. We were particularly interested in determining whether PKM2 directly interacts with FSTL1 in macrophages (figure 5A,B). Therefore, cell lysates were immunoprecipitated using anti-FSTL1 or anti-PKM2 antibodies, and the Co-IP complex was then immunoblotted. The results showed that FSTL1 bound to PKM2 in macrophages (figure 5C). In addition, confocal immunofluorescence analysis revealed that FSTL1 colocalised with PKM2 in the cytoplasm and nucleus (figure 5D). Next, we analysed the domains critical for the FSTL1-PKM2 interaction. According to the previously reported structural features of FSTL1 and PKM2, plasmids encoding four truncated fragments of FSTL1 each with ahemagglutinin (HA) tag and three truncated fragments of PKM2 each with a FLAG tag were constructed and transfected into 293 T cells (figure 5E).[32 33] Cell lysates were subjected to IP with an anti-HA antibody and immunoblotting with an anti-FLAG antibody. Our data showed that the FK domain of FSTL1 was critical for the interaction with the N-terminus or C-terminus of PKM2 (figure 5F). These results reveal that FSTL1 directly interacts with PKM2 through the FK domain of FSTL1 and the N-terminus or C-terminus of PKM2. Upregulation of the PKM2 protein in tissues was previously achieved by promoting transcription, inhibiting proteasome degradation or enhancing mRNA translation.[34] However, in this study, there were no significant differences in the PKM2 mRNA levels in the FSTL1-knockout or FSTL1-overexpressing cells (online supplemental figure 3). Thus, we speculated that FSTL1 might regulate the protein stability of PKM2. The results from a cycloheximide chase assay demonstrated that PKM2 in FSTL1-downregulated cells had a shorter half-life, while the half-life of PKM2 was much longer in the FSTL1-overexpressing cells than in the control cells (figure 5G). These results suggest that FSTL1 might regulate PKM2 stability by inhibiting proteasome degradation. Notably, we observed that the reduction in protein level of PKM2 accompanied by FSTL1 downregulation was recovered by the addition of MG-132 to the $FSTL1^{M\text{-}KO}$ and $FSTL1^{o/e}$ bone

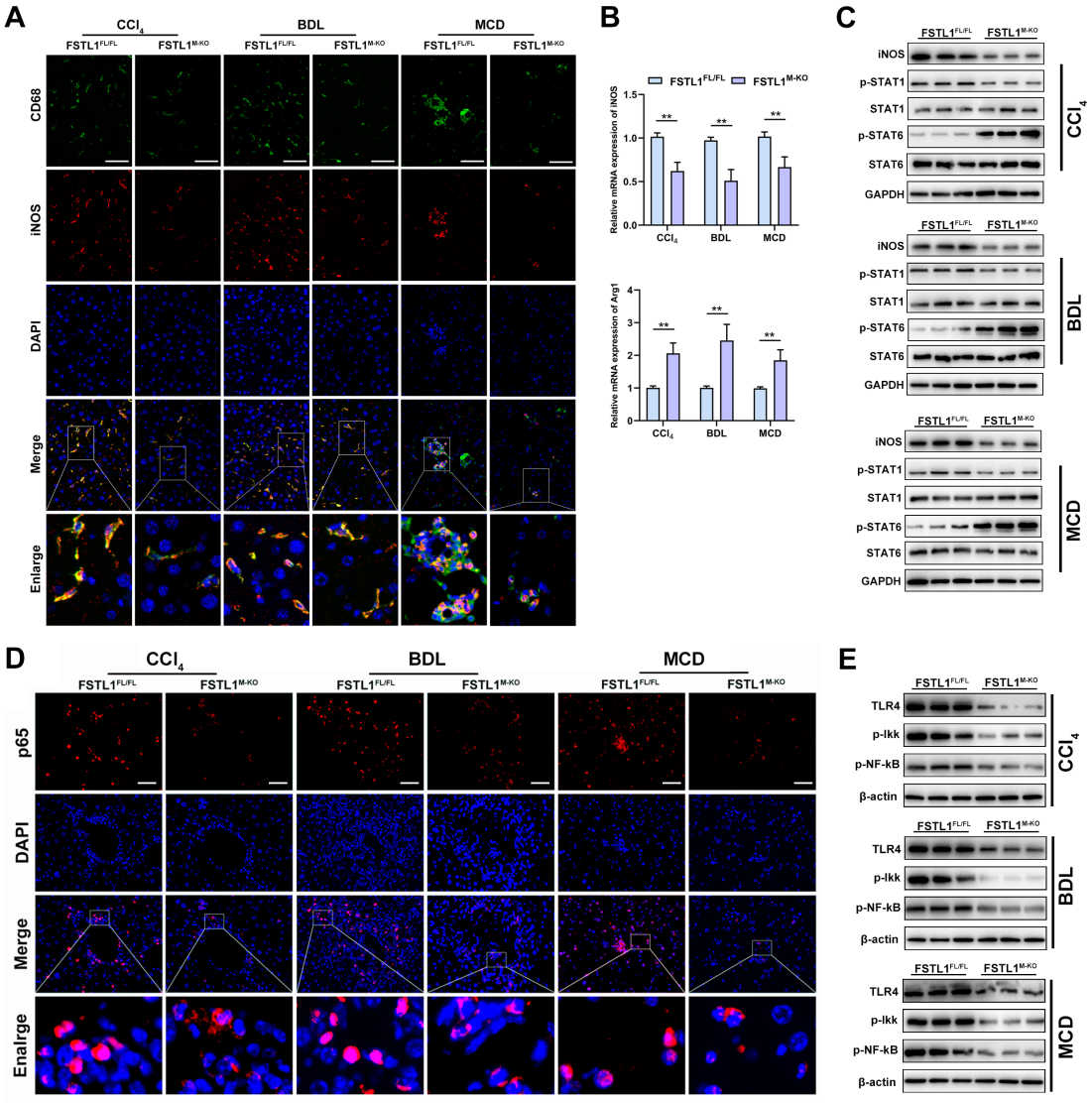

Figure 4 Myeloid follistatin-like protein 1 (FSTL1) deficiency suppresses M1 polarisation and nuclear factor kappa B (NF-κB) pathway activation in mice fibrotic livers. (A) Dual-immunofluorescence staining of inducible nitric oxide synthase (iNOS) and CD68 in liver tissues; (B) messenger RNA (mRNA) expression of iNOS and Arg1 was quantified in liver tissues; (C) protein expression of iNOS, p-STAT1, p-STAT6 and GAPDH were analysed in liver samples; (D) immunofluorescence staining of p65 and diamidino-2-phenylindole (DAPI) in liver tissues; (E) protein expression of toll-like receptor (TLR)-4, phospho-IkappaB kinases (p-Ikk), p-NF-κBp65 and GAPDH were analysed in liver samples. Data were presented as mean±SEM; n=6–8 per group; scale bars, 50 µm; **p<0.01. BDL, bile duct ligation; CCl_4, carbon tetrachloride; MCD, methionine-deficient and choline-deficient diet.

marrow-derived macrophages (BMDMs) cultures (figure 5H). Then, using an in vitro ubiquitination assay, we tested whether FSTL1 was involved in ubiquitin-mediated PKM2 degradation. Downregulation of FSTL1 increased the ubiquitination level of PKM2 protein in the $FSTL1^{M\text{-}KO}$ BMDMs. The ubiquitin-mediated degradation effect of PKM2 was significantly abrogated in FSTL1-overexpressing BMDMs (figure 5I). PKM2 ubiquitination is a critical step in PKM2 phosphorylation and nuclear translocation.

FSTL1 promotes PKM2 phosphorylation and nuclear translocation in macrophages of fibrotic liver tissues

To explore the role of PKM2 in FSTL1-mediated macrophage proinflammatory phenotype switching, we first examined whether PKM2 expression was altered in macrophages of fibrotic livers. Immunofluorescence staining showed that fibrotic livers had more $FSTL1^{+}$ macrophages (figure 6A, upper panel) and $PKM2^{+}$ macrophages (figure 6A, down panel) than control livers. Then, we analysed the protein expression of PKM2 and FSTL1 in the cytoplasm and nucleus of human liver samples, which showed the expression of PKM2 and FSTL1 was markedly increased in both the cytoplasm and nucleus of the fibrotic liver tissues (figure 6B and online supplemental figure 4). Immunofluorescence staining also displayed nuclear translocation of PKM2 and FSTL1 was significantly increased in the macrophages from patient livers compared with control livers (figure 6A, purple area). The results for the human fibrotic livers were similar to those for the mouse fibrotic livers. In contrast, disruption of myeloid FSTL1 clearly reduced $PKM2^{+}$ macrophages and hindered the nuclear import of PKM2 in liver macrophages compared with the $FSTL1^{FL/FL}$ mice (figure 6C). PKM2 phosphorylation was previously shown to be an indicator of monomer or dimer configuration, which can be translocated into the nucleus.[33 35] Therefore, we analysed the protein expression of total PKM2 and p-PKM2 in the cytoplasm and total PKM2 in the nucleus of

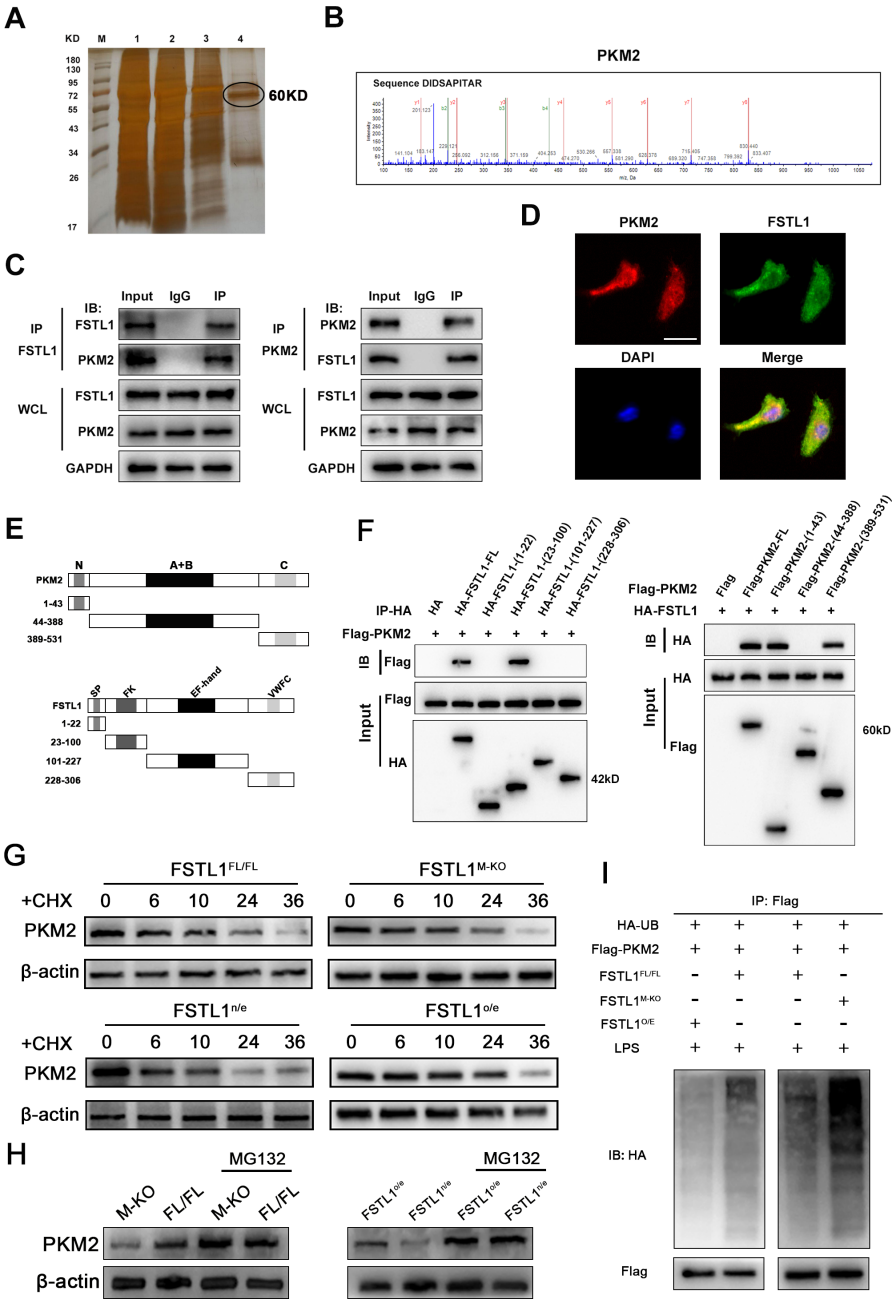

Figure 5 Follistatin-like protein 1 (FSTL1) directly binds with pyruvate kinase M2 (PKM2) and enhances the stability of PKM2 in macrophages. (A) The Co-immunoprecipitation (Co-IP) complex was subjected to silver-staining (line 4 represented the eluted protein); (B) the peptide sequences of the PKM2 protein as detected in the Co-IP complex by mass spectrometry; (C) western blot (WB) analysis of Co-IP complex confirmed that FSTL1 interacted with PKM2 in bone marrow-derived macrophages (BMDMs); (D) the immunofluorescence showed that FSTL1 colocalised with PKM2 and were expressed in both the cytoplasm and nucleus of BMDMs; (E) the structural compositions of FSTL1 and PKM2; (F) WB analysis of relationship between truncated FSTL1 and full-length PKM2 or truncated PKM2 and full-length FSTL1; (G) BMDMs extracted from $FSTL1^{FL/FL}$ and $FSTL1^{M\text{-}KO}$ mice and BMDMs extracted from $FSTL1^{FL/FL}$ transfected with LV-FSTL1 or lentivirus-negative control (LV-NC) were treated with cycloheximide (100 ng/mL) for the indicated periods of time; (H) BMDMs extracted from $FSTL1^{FL/FL}$ and $FSTL1^{M\text{-}KO}$ mice and BMDMs extracted from $FSTL1^{FL/FL}$ transfected with LV-FSTL1 or LV-NC were treated with or without MG132 (50 μM) for 6 hours. (I) In vitro ubiquitination assay of $FSTL1^{FL/FL}$, $FSTL1^{M\text{-}KO}$ and $FSTL1^{o/e}$ BMDMs. All cells were co-transfected with FLAG-PKM2 and HA-UB plasmid. Cell lysates were immunoprecipitated with anti-FLAG antibody followed by immunoblotting analysis with anti-HA or anti-FLAG antibody. Scale bars, 50 μm.

isolated liver macrophages. Figure 6D showed that, compared with the $FSTL1^{FL/FL}$ controls, FSTL1 deficiency reduced the expression of total PKM2 and p-PKM2 in the cytoplasm and then decreased total PKM2 in the nucleus. Collectively, these results indicate that macrophage FSTL1 promotes the nuclear translocation of PKM2.

FSTL1 deficiency attenuates the inflammatory responses, M1 polarisation and glycolysis in macrophages

To further analyse how FSTL1 regulates macrophage function in vitro, BMDMs were differentiated from $FSTL1^{FL/FL}$ or $FSTL1^{M\text{-}KO}$ mouse cells and subjected to lipopolysaccharide (LPS) stimulation. $FSTL1^{M\text{-}KO}$ macrophages showed decreased

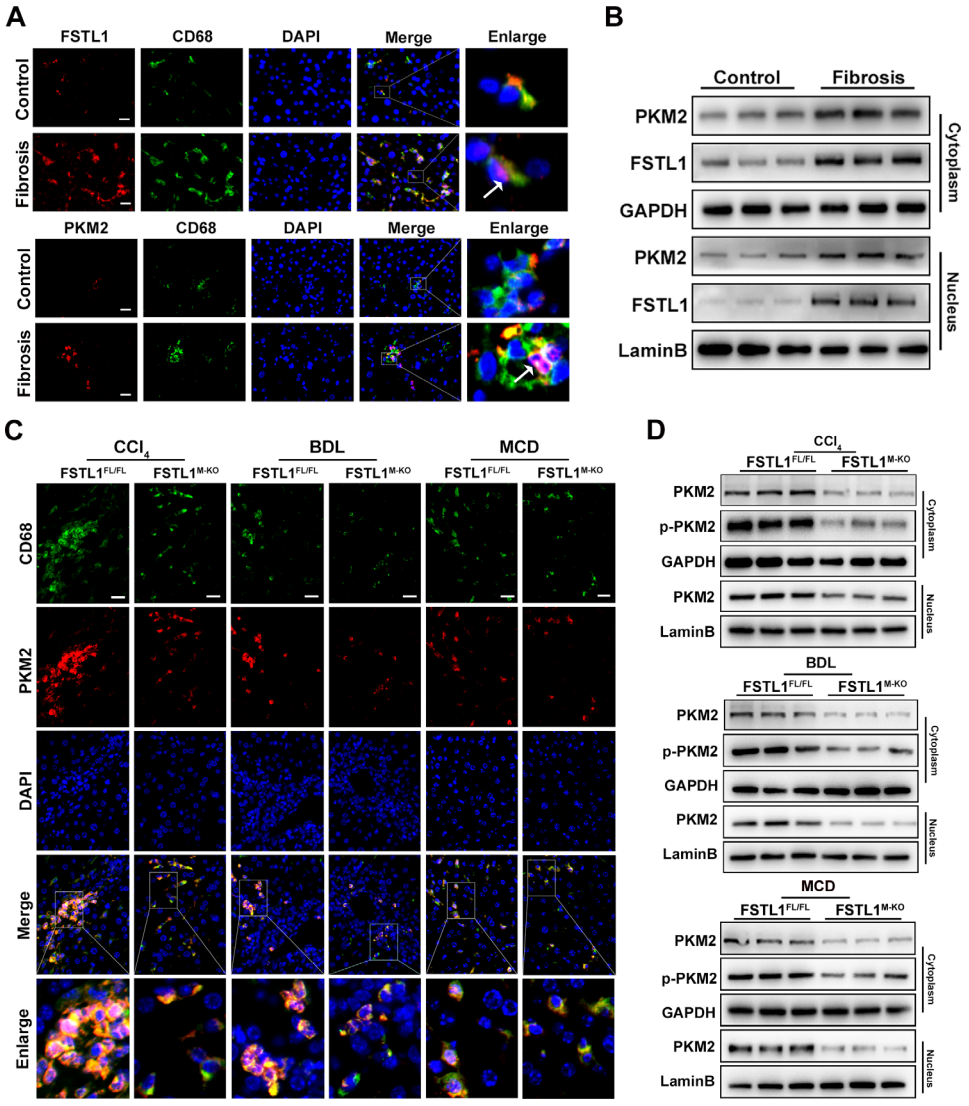

Figure 6 Follistatin-like protein 1 (FSTL1) promotes pyruvate kinase M2 (PKM2) phosphorylation and nuclear translocation in macrophage of fibrotic liver tissues. Human data (A–B) and mice data (C–D): (A) immunofluorescence staining of FSTL1 (upper panels) or PKM2 (lower panels), CD68 and DAPI in human liver tissues; (B) expressions of PKM2 and FSTL1 were analysed by western blot (WB) analysis in cytoplasm and nucleus of human livers; (C) immunofluorescence staining of PKM2, CD68 and DAPI in mice fibrotic livers; (D) expression of PKM2 and p-PKM2 were determined by WB analysis in cytoplasm and nucleus of fibrotic livers. Scale bars, 20 µm. BDL, bile duct ligation; CCl_4, carbon tetrachloride; MCD, methionine-deficient and choline-deficient diet.

expression of TNF-α and IL-1β and increased expression of IL-10 (figure 7A,B). Consistent with the in vivo experiments, FSTL1 deletion attenuated M1 polarisation and decreased TLR-4/NF-κB pathway activation in the BMDMs following LPS treatment (figure 7C–G). Next, we explored whether FSTL1 deficiency reduces PKM2 expression and nuclear translocation in vitro. PKM2 expression and its nuclear translocation were attenuated in the $FSTL1^{M\text{-}KO}$ BMDMs (figure 7C,D). PKM2 is crucial for the Warburg effect.[36] To explore whether FSTL1 also regulates glycolysis, we examined the extracellular acidification rate (ECAR) and relative lactate release level in these macrophages. We found that ECAR and lactic acid were markedly decreased after LPS stimulation in the $FSTL1^{M\text{-}KO}$ BMDMs compared with $FSTL1^{FL/FL}$ BMDMs (figure 7H,I). We used the glycolysis inhibitor 2-deoxy-D-glucose (2-DG) to block the glucose supply and found that the decrease in the expression of IL-1β and iNOS in $FSTL1^{M\text{-}KO}$ BMDMs was inhibited (figure 7J). In addition, we cocultured HSCs with BMDMs in an LPS-induced inflammatory environment (online supplemental figure 5A). FSTL1-deficient BMDMs markedly reduced α-SMA expression and attenuated the activation of HSCs (online supplemental figure 5B,C).

PKM2 activator inhibits FSTL1-mediated M1 polarisation and glycolysis in macrophages

To further determine the effect of PKM2 on FSTL1-induced macrophage polarisation and glycolysis, FSTL1-overexpressing ($FSTL1^{o/e}$) BMDMs were treated with the small-molecule PKM2 activator DASA-58.[37 38] DASA-58 alleviated $FSTL1^{o/e}$-induced TNF-α and IL-1β while increasing IL-10 level (figure 8A,B). As indicated by immunofluorescence staining of PKM2, iNOS and p65, inhibition of PKM2 nuclear translocation reversed FSTL1-induced macrophage M1 polarisation and NF-κB activation (figure 8C,D). These results were confirmed by WB analysis of PKM2, p-PKM2,

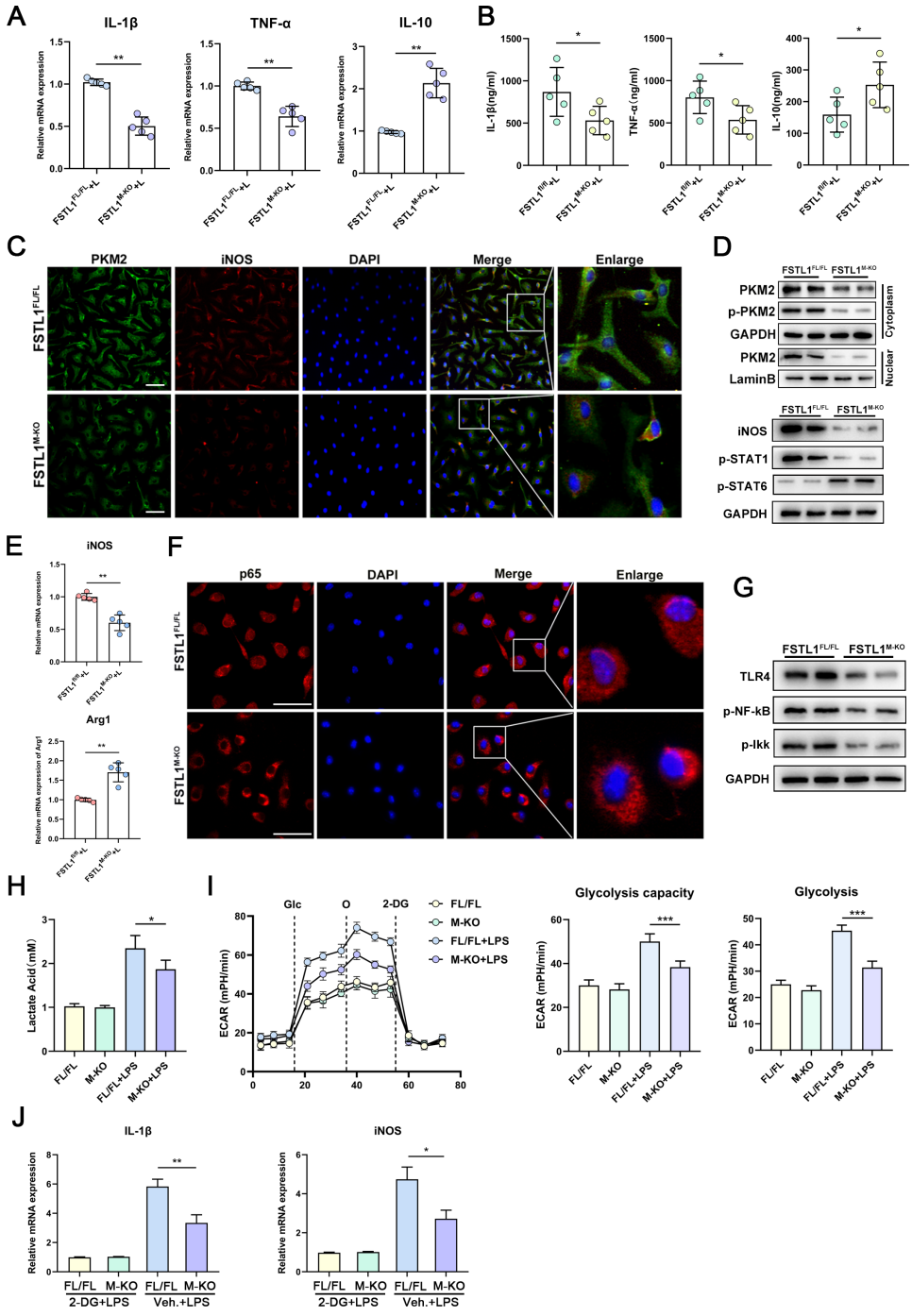

Figure 7 Follistatin-like protein 1 (FSTL1) deficiency attenuates inflammation and glycolysis in macrophages. Bone marrow-derived macrophages (BMDMs) treated with 100 ng/mL lipopolysaccharide (LPS) for 24 hours (A–G): (A–B) messenger RNA (mRNA) and protein expressions of tumour necrosis factor (TNF)-α, interleukin (IL)-1β and IL-10 were determined ; (C) immunofluorescence staining of pyruvate kinase M2 (PKM2) and inducible nitric oxide synthase (iNOS); (D) protein expression of PKM2, p-PKM2, iNOS, p-STAT1 and p-STAT6; (E) mRNA expression of iNOS and Arg1 was measured; (F) immunofluorescence staining of p65 and DAPI; (G) protein expression of toll-like receptor (TLR)-4, p-nuclear factor kappa B (NF-κB) and p-Ikk; (H) lactate acid production was measured from BMDMs in response to LPS (100 ng/mL, 6 hours). (I) Glycolytic rate and compacities of BMDMs were measured by real-time recording of extracellular acidification rates (ECAR) after successively injection of glucose (Glc), oligomycin (O) and 2-DG. (J) $FSTL1^{FL/FL}$ and $FSTL1^{M\text{-}KO}$ BMDMs treated with LPS (100 ng/mL, 4 hours). These cells were washed twice and pretreated with 10 mM 2-DG for 1 hour, followed by treatment with or without LPS (100 ng/mL) for another 4 hours. mRNA expression of IL-1β and iNOS were determined. Data were presented as mean±SEM of at least three independent experiments; scale bars, 50 μm; *p<0.05, **p<0.01, ***p<0.001.

iNOS, p-STAT1, p-STAT6, TLR-4, p-Ikk and p-p65 expression in the BMDMs (figure 8E–G). To further verify the role of PKM2 in FSTL1-mediated glycolysis, we examined the ECAR and relative lactate release level. ECAR and lactic acid were significantly higher in the $FSTL1^{o/e}$ BMDMs than in the $FSTL1^{n/e}$ BMDMs, and DASA-58 effectively reversed the $FSTL1^{o/e}$-induced increase in glycolysis (figure 8H,I). In addition, $FSTL1^{o/e}$-related proinflammatory mediators

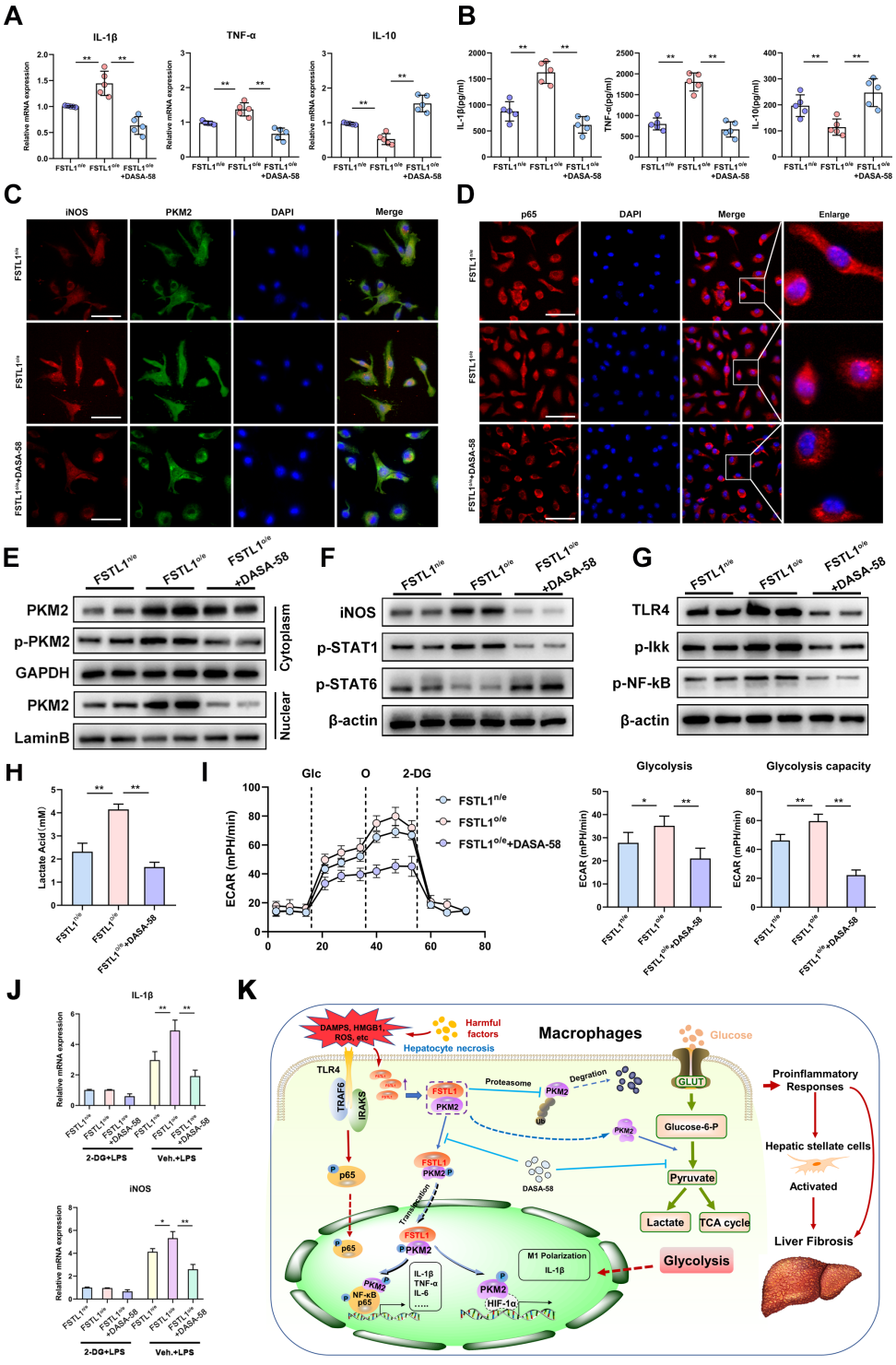

Figure 8 Pyruvate kinase M2 (PKM2) activator inhibits follistatin-like protein 1 (FSTL1)-mediated inflammation and glycolysis in macrophages. Bone marrow-derived macrophages (BMDMs) with FSTL1 overexpression (FSTL1$^{o/e}$) or normal expression (FSTL1$^{n/e}$) and FSTL1$^{o/e}$ BMDMs treated with DASA-58 (50 µM, 1 hour) were treated by lipopolysaccharide (LPS) stimulation. BMDMs treated with 100 ng/mL LPS for 24 hours (A–G): (A–B) messenger RNA (mRNA) expression and protein expressions of tumour necrosis factor (TNF)-α, interleukin (IL)-1β and IL-10 was determined; (C) dual-immunofluorescence staining of PKM2 and inducible nitric oxide synthase (iNOS); (D) protein expression of PKM2, p-PKM2, iNOS, p-STAT1 and p-STAT6; (E) mRNA expression of iNOS and Arg1 was measured; (F) immunofluorescence staining of p65 and DAPI; (G) protein expression of toll-like receptor (TLR)-4, p-nuclear factor kappa B (NF-κB) and p-Ikk. (H) Lactate acid production was measured from BMDMs in response to LPS (100 ng/mL, 6 hours). (I) Glycolytic rate and compacities of BMDMs were measured by real-time recording of extracellular acidification rates (ECAR) after successively injection of glucose (Glc), oligomycin (O) and 2-DG. (J) FSTL1$^{FL/FL}$ and FSTL1$^{M\text{-}KO}$ BMDMs treated with LPS (100 ng/mL) for 4 hours. These cells were washed twice and pretreated with 10 mM 2-DG for 1 hour, followed by treatment with or without LPS (100 ng/mL) for another 4 hours. mRNA levels or IL-1β and iNOS were determined. (K) Schematic illustration how FSTL1 complexed with PKM2 to promote phosphorylation and nuclear import of PKM2 and enhance cytoplasmic PKM2 stability in reprograming macrophage function during liver fibrosis. Data were presented as mean±SEM of at least three independent experiments; scale bars, 50 µm; *p<0.05, **p<0.01.

(IL-1β and iNOS) were neutralised by 2-DG (figure 8J). These results validate that the nuclear and cytoplasmic functions of PKM2 are crucial to FSTL1-induced M1 polarisation, glycolysis and inflammation.

DISCUSSION

To the best of our knowledge, this study is the first to document that FSTL1-mediated PKM2 is crucial for modulating macrophage function during liver fibrosis. The principal findings are as follows: (i) FSTL1 expression in macrophages is increased and is positively correlated with histological stages of liver fibrosis; (ii) myeloid FSTL1 deficiency suppresses M1 polarisation, reduces proinflammatory mediator expression and macrophage/neutrophil recruitment and alleviates liver fibrosis; (iii) FSTL1 directly binds to PKM2, inhibits ubiquitin-mediated degradation, enhances the stability of PKM2 and promotes PKM2 phosphorylation and nuclear translocation in macrophages and (iv) PKM2 is critical for FSTL1-mediated M1 polarisation, inflammation and glycolysis in macrophages. Our findings highlight the importance of FSTL1 as a key regulator of PKM2 function and inflammation in macrophages during liver fibrosis (figure 8K).

It has been reported that uncontrolled inflammation is a major driving force that transforms self-limited tissue repair processes to a vicious cycle, boosting the progression of liver fibrosis.[6] Macrophages are identified as pivotal regulators of liver inflammation that dominates the progression or resolution of liver fibrosis. Activated macrophages are generally divided into two categories, namely, M1 and M2.[39] M1-polarised macrophages disrupt local homeostasis and facilitate fibrosis by interacting with hepatocytes and other fibrosis-related non-parenchymal cells, such as HSCs.[8 39 40] FSTL1 is widely regarded as a proinflammatory gene possibly involved in macrophage polarisation.[19–21] It is reported that FSTL1 expression is enhanced in liver tissue and serum of patients with advanced fibrosis and steatosis.[41 42] Our data showed that FSTL1 expression is significantly increased in macrophages of human or mouse liver fibrotic tissues. In addition, we observed that myeloid FSTL1 deficiency inhibited macrophage TLR-4/NF-κB activation and M1 polarisation and limited hepatic inflammation and fibrosis.

FSTL1, as a secreted glycoproprotein, one widely acknowledged function of secreted FSTL1 is its modulatory role in inflammation, while the roles of FSTL1 in the cytoplasm and nucleus are not well understood. Circulatory FSTL1 levels are significantly elevated in patients with various autoimmune diseases.[43] Secreted FSTL1 has been shown to play modulatory roles in metabolism and glycolysis. $FSTL^{+/-}$ mice showed impaired energy expenditure and developed glucose intolerance with decreased adaptive thermogenesis of brown adipose tissue.[44] Furthermore, both acute and chronic infusion of FSTL1 impact oxygen consumption and energy substrate metabolism in cardiomyocytes through AMPK pathway activation.[45] These findings highlighted the modulatory role of FSTL1 in the inflammatory response and cellular metabolism of macrophages in a secretion-dependent manner. However, whether intracellular FSTL1 functions as a regulator of inflammation and cellular metabolism remains unknown.

One striking finding was that, through its FK domain, intracellular FSTL1 directly binds with the N-terminus or C-terminus of PKM2, which is a master immune regulator and established metabolic enzyme. PKM2 primarily exists as an enzymatically inactive form of monomer or dimer, with phosphorylation being the key indicator of its state.[33] Monomeric/dimeric PKM2 can translocate into the nucleus and stabilise the HIF-1α to promote the expression of glycolysis-related genes in tumours.[35] Furthermore, PKM2 directly promotes proinflammatory reprogramming of macrophages; it is upregulated by LPS stimulation and promotes IL-1β production by binding to its promoter, which predominantly occurs during glycolysis in M1 macrophages.[38] Herein, we found that the FSTL1 interacts with and stabilises the PKM2 protein by inhibiting PKM2 ubiquitin-mediated degradation. Our data further demonstrated that FSTL1 increases phosphorylation/nuclear PKM2, enhances PKM2-mediated M1 polarisation and promotes glycolysis in LPS-stimulated macrophages. It was reported that PKM2 can be directly bound to and phosphorylated by extracellular regulated kinase and translocated to the nucleus in a PIN1-dependent manner.[46] However, how FSTL1 promotes the phosphorylation and nuclear translocation of PKM2 is still unknown.

IL-1β expression is closely linked to Warburg metabolism in LPS-activated macrophages.[38 47] In addition, macrophage activation requires a metabolic switch from canonical oxidative phosphorylation towards glycolysis or the Warburg effect.[48] PKM2 is a pyruvate kinase that is widely regarded as a rate-limiting enzyme during glycolysis that catalyses the transfer of phosphate groups from phosphoenolpyruvate to ADP and produces pyruvate in the cytoplasm. Interestingly, we found that FSTL1 increased the expression and stability of PKM2 in the cytoplasm of macrophages following LPS treatment. Logically, our data indicated that FSTL1 deficiency reduced glycolysis after LPS stimulation. DASA-58, a highly specific small-molecule PKM2 activator, leads to a decrease in glycolytic and pentose phosphate pathway intermediates by activating the enzyme.[36] In addition, DASA-58 dramatically reverts this glycolytic phenotype in macrophages.[38] We found DASA-58 effectively restored $FSTL1^{o/e}$-mediated glycolysis, M1 polarisation and TLR-4/NF-κB pathway activation in LPS-stimulated macrophages. Thus, PKM2-mediated glycolysis is also critical for FSTL1-related M1 polarisation and inflammation. More importantly, the current study shows meticulously delineated FSTL1 regulation of glycolysis and glycolysis-dependent immune responses in macrophages, providing important insights into Warburg-like metabolic changes in macrophages.

In conclusion, we reveal the functional roles of macrophage FSTL1 in liver fibrosis. FSTL1 promotes M1 polarisation, glycolysis and the inflammatory response by binding to PKM2, promoting PKM2 phosphorylation and inhibiting PKM2 ubiquitination in macrophages. By identifying the molecular pathways by which FSTL1 mediates liver inflammation, our findings provide a rationale for novel therapeutic approaches to ameliorate macrophage-mediated liver inflammation and fibrosis.

Author affiliations
[1]Hepatobiliary Center of The First Affiliated Hospital, Nanjing Medical University; Research Unit of Liver Transplantation and Transplant Immunology, Chinese Academy of Medical Sciences, Nanjing, Jiangsu, China
[2]Jiangsu Key Lab of Cancer Biomarkers, Prevention and Treatment, Collaborative Innovation Center for Personalized Cancer Medicine, Nanjing Medical University, Nanjing, Jiangsu, China
[3]Jiangsu Collaborative Innovation Center of Biomedical Functional Materials, College of Chemistry and Materials Science, Nanjing Normal University, Nanjing, Jiangsu, China
[4]State Key Laboratory of Reproductive Medicine, Nanjing Medical University, Nanjing, Jiangsu, China

Contributors JR, HW and MN contributed equally. The study was designed by JR, FC and LL. The manuscript was written by JR, HW, FC and LL. The experiments and data analysis were performed by JR, HW, MN, ZW, ZW (5th author), SW, ML, PW, JQ, LZ, CW, HS, XW, FC and LL. JR, FC and LL supported and supervised the project. LL is the guarantor. All authors were involved in the critical revision of the manuscript.

Funding The project was supported by the National Natural Science Foundation of China (81871259, 81971495, and 82070675), the Foundation of Jiangsu

Collaborative Innovation Center of Biomedical Functional Materials, the Priority Academic Program Development of Jiangsu Higher Education Institutions, The Six talent peaks project in Jiangsu Province (2017-WSW-019) and the CAMS Innovation Fund for Medical Sciences (2019-I2M-5-035).

Competing interests None declared.

Patient consent for publication Not applicable.

Ethics approval The study design and sample collection protocols were approved by the Ethical Board of First Affiliated Hospital of Nanjing Medical University (Serial number: 2018-SRFA-197). All animal study protocols were approved by the Institutional Animal Care and Use Committee (IACUC) of Nanjing Medical University (AP#:GPTAP002). All patients provided informed consent at the time of recruitment.

Provenance and peer review Not commissioned; externally peer reviewed.

Data availability statement Data are available in a public, open access repository. A generic lab email address or an individual's ORCID identifier.

ORCID iDs
Jianhua Rao http://orcid.org/0000-0003-1222-7707
Xuehao Wang http://orcid.org/0000-0001-5849-0098
Ling Lu http://orcid.org/0000-0002-4983-5557

REFERENCES

1 Mokdad AA, Lopez AD, Shahraz S, *et al*. Liver cirrhosis mortality in 187 countries between 1980 and 2010: a systematic analysis. *BMC Med* 2014;12:145.
2 Tsochatzis EA, Bosch J, Burroughs AK. Liver cirrhosis. *Lancet* 2014;383:1749–61.
3 Hernandez-Gea V, Friedman SL. Pathogenesis of liver fibrosis. *Annu Rev Pathol* 2011;6:425–56.
4 Bataller R, Brenner DA. Liver fibrosis. *J Clin Invest* 2005;115:209–18.
5 Parola M, Pinzani M. Liver fibrosis: pathophysiology, pathogenetic targets and clinical issues. *Mol Aspects Med* 2019;65:37–55.
6 Pellicoro A, Ramachandran P, Iredale JP, *et al*. Liver fibrosis and repair: immune regulation of wound healing in a solid organ. *Nat Rev Immunol* 2014;14:181–94.
7 Koyama Y, Brenner DA. Liver inflammation and fibrosis. *J Clin Invest* 2017;127:55–64.
8 Tacke F, Zimmermann HW. Macrophage heterogeneity in liver injury and fibrosis. *J Hepatol* 2014;60:1090–6.
9 Tsuchida T, Friedman SL. Mechanisms of hepatic stellate cell activation. *Nat Rev Gastroenterol Hepatol* 2017;14:397–411.
10 Pradere J-P, Kluwe J, De Minicis S, *et al*. Hepatic macrophages but not dendritic cells contribute to liver fibrosis by promoting the survival of activated hepatic stellate cells in mice. *Hepatology* 2013;58:1461–73.
11 Hellerbrand C, Stefanovic B, Giordano F, *et al*. The role of TGFbeta1 in initiating hepatic stellate cell activation in vivo. *J Hepatol* 1999;30:77–87.
12 Seki E, De Minicis S, Osterreicher CH, *et al*. Tlr4 enhances TGF-beta signaling and hepatic fibrosis. *Nat Med* 2007;13:1324–32.
13 Miura K, Kodama Y, Inokuchi S, *et al*. Toll-Like receptor 9 promotes steatohepatitis by induction of interleukin-1beta in mice. *Gastroenterology* 2010;139:323–34.
14 Mattiotti A, Prakash S, Barnett P, *et al*. Follistatin-Like 1 in development and human diseases. *Cell Mol Life Sci* 2018;75:2339–54.
15 Geng Y, Dong Y, Yu M, *et al*. Follistatin-Like 1 (FSTL1) is a bone morphogenetic protein (BMP) 4 signaling antagonist in controlling mouse lung development. *Proc Natl Acad Sci U S A* 2011;108:7058–63.
16 Henkel M, Partyka J, Gregory AD, *et al*. FSTL-1 attenuation causes spontaneous Smoke-Resistant pulmonary emphysema. *Am J Respir Crit Care Med* 2020;201:934–45.
17 Peters MMC, Meijs TA, Gathier W, *et al*. Follistatin-Like 1 in cardiovascular disease and inflammation. *Mini Rev Med Chem* 2019;19:1379–89.
18 Chaly Y, Hostager B, Smith S, *et al*. Follistatin-Like protein 1 and its role in inflammation and inflammatory diseases. *Immunol Res* 2014;59:266–72.
19 Liu Y, Xu J, Liu T, *et al*. Fstl1 aggravates cigarette smoke-induced airway inflammation and airway remodeling by regulating autophagy. *BMC Pulm Med* 2021;21:45.
20 Li G, Ren H, Wu X, *et al*. Follistatin like protein-1 modulates macrophage polarization and aggravates dextran sodium sulfate-induced colitis. *Int Immunopharmacol* 2020;83:106456.
21 Chaly Y, Fu Y, Marinov A, *et al*. Follistatin-Like protein 1 enhances NLRP3 inflammasome-mediated IL-1β secretion from monocytes and macrophages. *Eur J Immunol* 2014;44:1467–79.
22 Zheng X, Qi C, Zhang S, *et al*. TGF-β1 induces Fstl1 via the Smad3-c-Jun pathway in lung fibroblasts. *Am J Physiol Lung Cell Mol Physiol* 2017;313:L240–51.
23 Dong Y, Geng Y, Li L, *et al*. Blocking follistatin-like 1 attenuates bleomycin-induced pulmonary fibrosis in mice. *J Exp Med* 2015;212:235–52.
24 Liu T, Liu Y, Miller M, *et al*. Autophagy plays a role in FSTL1-induced epithelial mesenchymal transition and airway remodeling in asthma. *Am J Physiol Lung Cell Mol Physiol* 2017;313:L27–40.
25 Zhou X, Xie F, Wang L, *et al*. The function and clinical application of extracellular vesicles in innate immune regulation. *Cell Mol Immunol* 2020;17:323–34.
26 Yang L, Xie M, Yang M, *et al*. Pkm2 regulates the Warburg effect and promotes HMGB1 release in sepsis. *Nat Commun* 2014;5:4436.
27 Moylan C, Diehl AM. Expression data for nonalcoholic fatty liver disease patients. gene expression omnibus, 2019. Available: https://www.ncbi.nlm.nih.gov/geo/query/acc.cgi?acc=GSE49541
28 Mas VR, Maluf DG, Archer KJ. RMA expression data for liver samples from subjects with HCV, HCV-HCC, or normal liver. gene expression omnibus, 2018. Available: https://www.ncbi.nlm.nih.gov/geo/query/acc.cgi?acc=GSE14323
29 Lalloyer F, Bauge E, Pawlak M. Transcriptomic analysis of CLL4-induced liver injury in WT and DpT KO mice. gene expression omnibus, 2019. Available: https://www.ncbi.nlm.nih.gov/geo/query/acc.cgi?acc=GSE141821
30 Misu H, Takamura T. Expression data from mouse liver treated with metformin. gene expression omnibus, 2019. Available: https://www.ncbi.nlm.nih.gov/geo/query/acc.cgi?acc=GSE35961
31 Gijbels E, Devisscher L, Vinken M. Robustness testing and optimization of an adverse outcome pathway on cholestatic liver injury. gene expression omnibus, 2020. Available: https://www.ncbi.nlm.nih.gov/geo/query/acc.cgi?acc=GSE15249432
32 Li X, Li L, Chang Y, *et al*. Structural and functional study of FK domain of FSTL1. *Protein Sci* 2019;28:1819–29.
33 Wang P, Sun C, Zhu T, *et al*. Structural insight into mechanisms for dynamic regulation of PKM2. *Protein Cell* 2015;6:275–87.
34 Dayton TL, Jacks T, Vander Heiden MG. Pkm2, cancer metabolism, and the road ahead. *EMBO Rep* 2016;17:1721–30.
35 Luo W, Hu H, Chang R, *et al*. Pyruvate kinase M2 is a PHD3-stimulated coactivator for hypoxia-inducible factor 1. *Cell* 2011;145:732–44.
36 Anastasiou D, Yu Y, Israelsen WJ, *et al*. Pyruvate kinase M2 activators promote tetramer formation and suppress tumorigenesis. *Nat Chem Biol* 2012;8:839–47.
37 Guo J, Ren R, Yao X, *et al*. Pkm2 suppresses osteogenesis and facilitates adipogenesis by regulating β-catenin signaling and mitochondrial fusion and fission. *Aging* 2020;12:3976–92.
38 Palsson-McDermott EM, Curtis AM, Goel G, *et al*. Pyruvate kinase M2 regulates HIF-1α activity and IL-1β induction and is a critical determinant of the Warburg effect in LPS-activated macrophages. *Cell Metab* 2015;21:65–80.
39 Xu R, Zhang Z, Wang F-S. Liver fibrosis: mechanisms of immune-mediated liver injury. *Cell Mol Immunol* 2012;9:296–301.
40 Sica A, Invernizzi P, Mantovani A. Macrophage plasticity and polarization in liver homeostasis and pathology. *Hepatology* 2014;59:2034–42.
41 Ramnath D, Irvine KM, Lukowski SW, *et al*. Hepatic expression profiling identifies steatosis-independent and steatosis-driven advanced fibrosis genes. *JCI Insight* 2018;3:e120274.
42 Ramachandran P, Dobie R, Wilson-Kanamori JR, *et al*. Resolving the fibrotic niche of human liver cirrhosis at single-cell level. *Nature* 2019;575): :512–8.
43 Li D, Wang Y, Xu N, *et al*. Follistatin-Like protein 1 is elevated in systemic autoimmune diseases and correlated with disease activity in patients with rheumatoid arthritis. *Arthritis Res Ther* 2011;13:R17.
44 Fang D, Shi X, Lu T, *et al*. The glycoprotein follistatin-like 1 promotes brown adipose thermogenesis. *Metabolism* 2019;98:16–26.
45 Seki M, Powers JC, Maruyama S, *et al*. Acute and chronic increases of circulating FSTL1 normalize energy substrate metabolism in pacing-induced heart failure. *Circ Heart Fail* 2018;11:e004486.
46 Yang W, Zheng Y, Xia Y, *et al*. Erk1/2-Dependent phosphorylation and nuclear translocation of PKM2 promotes the Warburg effect. *Nat Cell Biol* 2012;14:1295–304.
47 Tannahill GM, Curtis AM, Adamik J, *et al*. Succinate is an inflammatory signal that induces IL-1β through HIF-1α. *Nature* 2013;496:238–42.
48 Kelly B, O'Neill LAJ. Metabolic reprogramming in macrophages and dendritic cells in innate immunity. *Cell Res* 2015;25:771–84.

Supplemental table 1. Baseline characteristics of included patients.

Fibrosis stage	Normal histology	Mild fibrosis (20)			Advanced fibrosis (13)		
		HBV (1-4)	HCV (1-2)	NASH (1-2)	HBV (5-6)	HCV (3-4)	NASH (3-4)
Patients number	18	HBV (8)	HCV (9)	NASH (3)	HBV (4)	HCV (8)	NASH (1)
Age (age)	46.6±6.2	54.8±9.0	46.8±6.6	52.0±2.2	58.3±5.4	56.8±9.1	51.0
Serum TB (umol/L)	7.9±3.0	16.7±5.5	14.5±4.5	13.3±4.3	21.0±4.7	18.8±3.2	22.4
Serum ALT (U/L)	18.1±9.1	58.0±18.2	65.9±36.0	55.7±18.4	103.5±26.5	78.9±24.8	66.0
Serum AST (U/L)	23.1±10.3	64.5±22.7	57.9±26.8	45.0±8.8	80.5±7.0	76.0±33.1	78.0
Serum ALB (g/L)	41.6±1.8	39.1±1.9	40.7±2.6	39.2±1.4	35.4±2.1	34.8±2.1	35.6

Hepatic fibrosis stage in patients with HBV infection was defined as Ishak fibrosis score, 1-4 for Mild fibrosis, 5-6 for Advanced fibrosis.[1-4] Hepatic fibrosis stage in patients with HCV infection was defined as Metavir score, 1-2 for Mild fibrosis, 3-4 for Advanced fibrosis.[3-5] Hepatic fibrosis stage in patients with NASH was defined as NAFLD activity score, 1-2 for Mild fibrosis, 3-4 for Advanced fibrosis.[6-8] Quantitative variables are in mean±SD. HBV, Hepatitis B virus; HCV, Hepatitis C virus; NASH, non-alcoholic steatohepatitis; ALB, albumin; ALT, alanine aminotransferase; AST, aspartate aminotransferase; TB, total bilirubin.

Supplemental table 2. Hepatic fibrosis stage in patients with HBV infection was defined as Ishak fibrosis score.

Fibrosis stage (Ishaks)	1	2	3	4	5	6
Patients number	3	2	2	1	1	3
Age (age)	47.3±4.0	57.5±1.5	59.5±12.5	62	65	56±4.2
Serum total bilirubin (umol/L)	10.9±3.0	16.7±3.0	22.1±0.2	23.2	23.6	20.1±5.1
Serum ALT (U/L)	44.7±19.0	61.0±6.0	62.0±11.0	84.0	121	97.7±28.2
Serum AST (U/L)	56.7±32.3	66.5±11.5	68.0±13.0	77.0	82.0	80.0±8.0
Serum albumin (g/L)	40.9±1.1	38.3±1.9	38.3±0.4	36.9	35.6	35.3±2.5

Supplemental table 3. Hepatic fibrosis stage in patients with HCV infection was defined as Metavir score

Fibrosis stage (Metavir)	1	2	3	4
Patients number	6	3	3	5
Age (age)	45.8±7.3	51.3±2.9	56.7±5.4	56.8±10.7
Serum total bilirubin (umol/L)	12.7±4.0	18.2±2.9	19.8±2.5	18.1±3.4
Serum ALT (U/L)	60.3±39.7	76.5±28.5	80.0±18.6	78.0±28.0
Serum AST (U/L)	55.8±31.8	62.0±10.0	74.0±37.0	77.2±30.4
Serum albumin (g/L)	41.6±2.6	39.1±1.4	35.7±1.7	34.2±2.1

Supplemental table 4. Hepatic fibrosis stage in patients with NASH was defined as NAFLD activity score

Fibrosis stage (NAS)	1	2	3	4
Patients number	2	1	0	1
Age (age)	51.0±2.0	54	——	51
Serum total bilirubin (umol/L)	12.3±5.0	15.5	——	22.4
Serum ALT (U/L)	53.0±22.0	61	——	66
Serum AST (U/L)	46.5±10.5	42	——	78
Serum albumin (g/L)	40.1±0.6	37.3	——	35.6

Supplemental table 5. Primers for mice genotyping

Primer name	Target	No	Lot	Direction	Sequence	wt	ko	Blast	PRI	Using	Method	Cite
TL-CRE-G-JCYK-K	Lyz2Mut	C66	1	Reverse	5’-CCCAGAAATGCCAGATTACG-3’	_	750-bp	N		Genomic DNA	Age	JYCK
		C67		Forward	5’-CTTGGGCTGCCAGAATTTCTC-3’					Tail		
TL-CRE-G-JCYK-W	Lyz2WT	C67	1	Reverse	5’-CTTGGGCTGCCAGAATTTCTC-3’	350-bp	_	Y		Genomic DNA	Age	JYCK
		C68		Forward	5’-TTACAGTCGGCCAGGCTGAC-3’					Tail		
NM-FSTL1-G-JYCK-FL	FSTL1-FLOX	FI34F-1	1	Reverse	5’-ACATGGTGACCATCCTTCGG-3’	547	734			Genomic DNA	Age	JYCK
		FI34R-1		Forward	5’TTCTAGGTTCCTCCTAAAAC-3’					Tail		

Supplemental table 6. Primer sequences for the amplification.

Gene	Forward Primer（5′ → 3′）	Reverse Primer（5′ → 3′）
FSTL1(Human)	GCCATGACCTGTGACGGAAA	CAGCGCTGAAGTGGAGAAGA
Collagen I (Human)	GAGGGCCAAGACGAAGACATC	CAGATCACGTCATCGCACAAC
TIMP-1 (Human)	CTTCTGCAATTCCGACCTCGT	CCCTAAGGCTTGGAACCCTTT
β-actin(Human)	CATGTACGTTGCTATCCAGGC	CTCCTTAATGTCACGCACGAT
α-SMA(Mouse)	GTCCCAGACATCAGGGAGTAA	TCGGATACTTCAGCGTCAGGA
Collagen-I (Mouse)	GCTCCTCTTAGGGGCCACT	CCACGTCTCACCATTGGGG
TIMP-1 (Mouse)	GCAACTCGGACCTGGTCATAA	CGGCCCGTGATGAGAAACT
β-actin (Mouse)	GGCTGTATTCCCCTCCATCG	CCAGTTGGTAACAATGCCATGT
TNF-α (Mouse)	GCCAGAGGGCTGATTAGAGA	CAGCCTCTTCTCCTTCCTGAT
IL-1β (Mouse)	CCAGGATGAGGACCCAAGCA	TCCCGACCATTGCTGTTTCC
IL-10 (Mouse)	ACAGGGAAGAAATCGATGACA	TGGGGGAGAACCTGAAGAC
iNOS (Mouse)	AATCTTGGAGCGAGTTGTGG	CAGGAAGTAGGTGAGGGCTTG
Argines1 (Mouse)	CTCCAAGCCAAAGTCCTTAGAG	AGGAGCTGTCATTAGGGACATC
TGF-β (Mouse)	CGCCATCTATGAGAAAACCAA	GAGTTCCACATGTTGCTCCA

References

1. Sun, Y., et al., *Persistent Low Level of Hepatitis B Virus Promotes Fibrosis Progression During Therapy.* Clin Gastroenterol Hepatol, 2020. **18**(11): p. 2582-2591 e6.
2. Sterling, R.K., et al., *Evaluating Noninvasive Markers to Identify Advanced Fibrosis by Liver Biopsy in HBV/HIV Co-infected Adults.* Hepatology, 2020. **71**(2): p. 411-421.
3. Patin, E., et al., *Genome-wide association study identifies variants associated with progression of liver fibrosis from HCV infection.* Gastroenterology, 2012. **143**(5): p. 1244-1252 e12.
4. Cacoub, P., et al., *Comparison of non-invasive liver fibrosis biomarkers in HIV/HCV co-infected patients: the fibrovic study--ANRS HC02.* J Hepatol, 2008. **48**(5): p. 765-73.
5. Konerman, M.A., et al., *Fibrosis progression in human immunodeficiency virus/hepatitis C virus coinfected adults: prospective analysis of 435 liver biopsy pairs.* Hepatology, 2014. **59**(3): p. 767-75.
6. Kleiner, D.E., et al., *Design and validation of a histological scoring system for nonalcoholic fatty liver disease.* Hepatology, 2005. **41**(6): p. 1313-21.
7. Newsome, P.N., et al., *FibroScan-AST (FAST) score for the non-invasive identification of patients with non-alcoholic steatohepatitis with significant activity and fibrosis: a prospective derivation and global validation study.* Lancet Gastroenterol Hepatol, 2020. **5**(4): p. 362-373.
8. Harrison, S.A., et al., *NGM282 Improves Liver Fibrosis and Histology in 12 Weeks in Patients With Nonalcoholic Steatohepatitis.*

Hepatology, 2020. **71**(4): p. 1198-1212.

Supplement Materials

Methods

Construction of myeloid-specific FSTL1 deficient mice

FSTL1$^{FL/FL}$ (carrying the a floxed allele) and Lyz2-Cre (expressing the Cre recombinase specifically in myeloid cells) mice were both acquired from GemPharmatech. Co. Ltd (Nanjing, China). FSTL1 conditional konckout mice were made via CRISPR/Cas9 system. Firstly, two sgRNAs-targeting the introns on both sides of the floxed region of FSTL1 were respectively constructed and transcribed invitro. And the donor vector with the loxp fragment was designed and constructed in vitro. Then Cas9 mRNA, sgRNA and donor will be co-injected into zygotes. Thereafter, the zygotes were transferred into the oviduct of pseudopregnant ICR females at 0.5 dpc. And F0 mice was birthed after 19~21 days of transplantation, all the offsprings of ICR females (F0 mice) were identified by PCR and sequencing of tail DNA. And positive F0 mice were genetyped by the methods. Finally, crossing F0 mice with C57BL/6J mouse to build up heterozygous mice (FSTL1$^{FL/WT}$). A stable F1 generation mouse model was obtained by mating positive F0 generation mice with C57BL/6J mice.

For producing myeloid-specific knockout mice, homozygous FSTL1$^{FL/FL}$ mice were bred with homozygous Lyz2-Cre mice, and their heterozygous offspring were back-crossed with homozygous FSTL1$^{FL/FL}$ mice (supplemental figure 6). Mice were genotyped using primers listed in supplemental table 5.

Protein extraction and western blot

Protein extraction was performed to extracted nuclear or cytoplasmic protein according to manufacturer's instruction (P0027, Beyotime Biotechnology, Shanghai, China). Western blot was performed as described previously [1]. Briefly, samples were lysed using RIPA solution. BCA were used to normalize protein concentrations between samples. Thermal denatured protein samples were subjected to 12% SDS-polyacrylamide gel electrophoresis and were then transferred to a PVDF membrane (Bio-Rad, Hercules, CA) for antibody incubation.

Antibodies

Primary antibodies used in this study were as follows: rabbit anti-FSTL1 mAb (ab223287, Abcam); rabbit anti-PKM2 mAb (4053S, Cell Signaling Technology); mouse anti-PKM2 mAb (60268-1-Ig, Proteintech); rabbit anti-p-PKM2 mAb (3827, Cell Signaling Technology); rabbit anti-p-STAT6 mAb (56554S, Cell Signaling Technology); rabbit anti-p-STAT1 mAb (9167S, Cell Signaling Technology); rabbit anti-iNOS mAb (13120S, Cell Signaling Technology); rabbit anti-TLR4 mAb (14358S, Cell Signaling Technology); rabbit anti-p65 mAb (8242S, Cell Signaling Technology); rabbit anti-p-NF-kB mAb (3033S, Cell Signaling Technology); rabbit anti-p-Ikk mAb (2697S, Cell Signaling Technology); rat anti-CD68 mAb (ab53444, Abcam); rat anti-F4/80 mAb (ab6640, Abcam); rabbit anti α-SMA mAb (19245S, Cell Signaling Technology); rabbit anti-Ly6G mAb (87048S, Cell Signaling Technology); recombinant rabbit anti-GAPDH mAb (ab181602, Abcam); recombinant rabbit IgG isotype control (ab172730, Abcam); rabbit IgG isotype control (3452S, Cell Signaling Technology); rabbit anti-flag-Tag mAb (14793, Cell Signaling Technology); rabbit anti-myc-Tag mAb (2276S, Cell Signaling Technology).

Secondary antibodies used in this study were as follows: HRP-conjugated goat Anti-Rabbit IgG (ab205718, Abcam); HRP-conjugated goat Anti-Rat IgG (ab205720, Abcam); HRP-conjugated goat Anti-Mouse IgG (ab205719, Abcam); Alexa Fluor 488-conjugated goat anti-Mouse IgG (A-11001, Invitrogen); Alexa Fluor 488-conjugated goat anti-Rabbit IgG (A-11008, Invitrogen); Alexa Fluor 488-conjugated goat anti-Rat IgG (A-11006, Invitrogen); Alexa Fluor 594-conjugated goat anti-Mouse IgG (A-11005, Invitrogen); Alexa Fluor 594-conjugated goat anti-Rabbit IgG (A-11012, Invitrogen); Alexa Fluor 594-conjugated goat anti-Rat IgG (A-11007, Invitrogen).

Plasmid construction and transfection

Expression plasmid constructs, including pcDNA3.1(+)-HA-FSTL1, pcDNA3.1(+)-HA-FSTL1-SP domain deletion, pcDNA3.1(+)-HA-FSTL1-FK domain (follistatin-like and kazal-like Domain) deletion, pcDNA3.1(+)-HA-FSTL1-EF-hand domain deletion, pcDNA3.1(+)-HA-FSTL1-VWFC domain deletion, pcDNA3.1(+)-Flag-PKM2, pcDNA3.1(+)-Flag-PKM2-AB-domain deletion, pcDNA3.1(+)-FlagPKM2-C-domain deletion, pcDNA3.1(+)-Flag-PKM2-N-domain deletion were all constructed and

purchased from Shanghai (GenePharma, Shanghai, China). Lipofectamine 3000 (Invitrogen, Carlsbad, CA) was used to transfect. Briefly, 293T cells were plated in a 6-well plate (3 x105 cells/well). After 24h, the 293T cells were transfected with 2.5 mg/well plasmid, 5 ml Lipo 3000 and 5 ml P3000. Empty pcDNA3.1(+)-vector was added into each well to equalize total amounts of transfected plasmids.

Co-immunoprecipitation and mass spectrometry

Immunoprecipitation and mass spectrometry were performed as previously described [1]. Briefly, harvested cell lysates were incubated with the specific primary antibodies overnight at 4°C, and conjugated with protein A/G beads (Santa Cruz Biotechnology, CA) for 4-6 h. After washing, immunoprecipitants were boiled in Laemmli sample buffer for 10 min. The immunoprecipitated proteins was detected by western blot or reverse phase liquid chromatography/mass spectrometry (RPLC/MS)-ESI-Q-ToFQ analyzer (TripleTOF 6600 MS system, Applied Biosystem, USA).

Quantitative real-time PCR

Total RNA was extracted from tissue samples or cells with TRIzol reagent (Invitrogen) followed by isopropyl alcohol precipitation. RNA concentration and quality were evaluated using Nano-drop system and was then reverse-transcribed into cDNA by commercially available kit (Vazyme, Nanjing, China). SYBR-green based real-time quantitative PCR kits (Vazyme, Nanjing, China) were used to perform mRNA quantification. Gene expressions were normalized to β-actin expression. Primer sequences are listed in supplemental table 6.

Biochemical analysis

Secreted cytokines (IL-1β, IL-10 and TNF-α) were measured using ELISA kits (eBioscience, San Diego, CA), according to manufacturer's instruction. To measure serum alanine transaminase (ALT), aspartate transaminase (AST), albumin (ALB), and total bilirubin (TB) automated chemical analyzer (Olympus, Tokyo, Japan) was used.

Immunohistochemistry and Immunofluorescence (IF) staining

Formaldehyde-fixed, paraffin-embedded liver samples were sectioned into 4μm slides. Immunohistochemistry staining and immunofluorescence (IF) staining were performed as previously described [1]. Briefly, for tissue samples, formaldehyde-fixed, paraffin-

embedded slides were subjected to dewaxing, hydration and antigen retrieval, followed by blocking and antibody incubation. For *in vitro* experiments, cells were seeded on coverslips and were fixed with 3% paraformaldehyde, permeated with 0.1% Triton X-100 followed by 10% BSA blockage. Primary antibodies were diluted as suggested, added onto slides and were incubated at 4℃ overnight in a moist chamber. Then slides were washed with PBS and incubated with 488-/594-/HRP-conjugated secondary antibodies. For IF staining, slides were further incubated with DAPI (Invitrogen) and mounted in IF mounting medium (Servicebio). Bright field and fluorescence microscopy were performed using an Olympus BX53 system. Quantification of the mean fluorescence intensity was performed with the ImageJ software under least three randomly selected fields (supplemental figure 8). Nuclei were stained with DAPI, and the percentage of nuclear p65 and PKM2 positive cells was counted under least three randomly selected fields (supplemental figure 8). Confocal microscopy was performed using Olympus FV3000 confocal microscopy system.

Primary cell isolation, culture and treatment

Recombinant M-CSF (PeproTech, USA) were used to differentiate bone marrow-derived macrophages (BMDMs) as previously described [1]. Briefly, femurs and tibias were carefully dislodged from sacrificed 8~12 weeks-old male mice in a laminar flow hood. Bone marrow cells were then flushed out using 30 G needle on a 20 mL syringe filled with DMEM. After red blood lysis using LCK buffer solution (Beyotime), cells were washed with PBS and seeded in DMEM medium containing 20 ng/mL M-CSF and 10% fetal bovine serum (FBS). After 4-day cultivation, cells were washed with PBS and changed with new medium. Cells were regarded as fully differentiated BMDMs on day 7. Liver macrophages were isolated from mice by portal perfusion using pre-warmed solution containing 0.05% collagenase type IV dissolved in Ca^{2+}/Mg^{2+} HBSS, filtered through a 40μm nylon strainer (Falcon) and were then subjected to 40 g centrifugation without brake. Primary hepatocytes were separated using 50% Percoll gradient by 200 g centrifugation and were seeded in DMEM medium supplemented with 10% FBS. To enrich liver macrophages, NPCs (nonparenchymal cells) were suspended in HBSS and layered onto a two-layer 25%-

50% Percoll gradient (Sigma-Aldrich, St. Louis, MO) in a 50-ml conical centrifuge tube and centrifuged at 1800g at 4°C for 15 min. Liver macrophages in the middle layer were collected and allowed to attach to cell culture plates in supplemented DMEM with 10% FBS for 20 min at 37°C. Nonadherent cells were removed by replacing the culture medium. The purity of macrophages in the adherent cells was determined by immunofluorescent staining with anti-F4/80. 80-90% adherent cells were F4/80 positive (Supplemental figure 7A). Cell viability was assessed after 0 or 24 h using a Countess II FL Automated Cell Counter (Thermo Fisher, USA) with trypan blue exclusion (Supplemental figure 7B). HSC-T6 cells purchased from the Cell Center of Shanghai Institutes for Biological Sciences. HSC-T6 cells were cultured in DMEM medium supplemented with 10% FBS. BMDMs plasmid transfection was performed using Lipofectamine 3000 (Invitrogen, Carlsbad, CA). Adenoviruses (GenePharma, Shanghai, China) expressing FSTL1 and vector were used to transfect BMDMs for 48h on day 0~2 of cultivation. Cells were then treated with LPS at the concentration of 100 ng/mL (Sigma, St. Louis, MO) for 24 h.

BMDMs Co-culture with HSCs

BMDMs were co-cultured with HSCs at 1:1 using DMEM with 10% FBS. The co-cultures were performed in six-well plates with HSCs seeded at lower chamber. BMDMs were seeded onto 0.4 μm pore-size Transwell culture inserts (BD Biosciences). Co-cultures were then treated with 100ng/ml lipopolysaccharide (LPS) for 24 hours.

Bioinformatics analysis using publicly available datasets

All bioinformatics analysis were performed under *R* environment version 4.0.2. Publicly available omics data were provided by Gene Expression Omnibus (GEO). Several datasets characterizing liver gene expression using *Affymetrix*™ expression microarrays were analyzed. In dataset GSE141821, mice were treated with CCL_4 (n = 9) or olive oil (control, n = 8) for 8 weeks [2]. In dataset GSE35961, mice were fed with high fat, methionine- and choline-deficient diet for 8 weeks (n= 4 per group) [3]. In dataset GSE152494, mice were subjected to common bile duct ligation or sham operation and samples were harvested after 6 weeks (n = 6 per group) [4]. In dataset GSE49541, liver samples were obtained from 72 patients with NASH-associated

fibrosis (40 with fibrosis stage F0 - F1 and 32 with F3 - F4) [5]. In dataset GSE14323, 41 cirrhotic human liver samples and 19 control samples were analyzed [6]. R package *Affy* were used to preprocess data. R package *limma* were used to identify differentially over-expressed genes, with threshold defined as $\log_2$-fold change > 2 and adjusted *P* value < 0.01. Pre-processed sparse matrix files were loaded using *Seurat* R package. Genes expressed in fewer than three cells in a sample were excluded. Cells that 1) had fewer than 300 genes, 2) mitochondrial gene content >30% of total UMI count were excluded. Data were normalized and log-transformed using function *NormalizeData* with scale factor = 10,000.

Extracellular acidification rate monitoring

Seahorse XF-24 Extracellular Flux Analyzer (Agilent) was used for real-time recording of extracellular acidification rate (ECAR). Briefly, FL/FL and M-KO BMDMs extracted from mice were seeded in Seahorse XF-24 microplates ($1.5x10^5$ cells/well) treated with/without LPS (100 ng/mL) for 6 h. Before analysis, the cells were switched into ECAR media for 1 h at 37°C. After baseline measurements, 10 mM glucose, 1 μM oligomycin, and 50 mM 2-DG were sequentially injected into each well at indicated time points.

Extracellular lactate assay

Extracellular levels of lactate were determined using lactate assay kit (BioVision) according to the manufacturer's instructions.

References

1. Rao, J., et al., *Nogo-B is a key mediator of hepatic ischemia and reperfusion injury.* Redox Biol, 2020. **37**: p. 101745.
2. Lefebvre, P., et al., *Interspecies NASH disease activity whole-genome profiling identifies a fibrogenic role of PPARalpha-regulated dermatopontin.* JCI Insight, 2017. **2**(13).
3. Kita, Y., et al., *Metformin prevents and reverses inflammation in a non-diabetic mouse model of nonalcoholic steatohepatitis.* PLoS One, 2012. **7**(9): p. e43056.
4. Gijbels, E., et al., *Robustness testing and optimization of an adverse outcome pathway on cholestatic liver injury.* Arch Toxicol, 2020. **94**(4): p. 1151-1172.
5. Moylan, C.A., et al., *Hepatic gene expression profiles differentiate presymptomatic patients with mild versus severe nonalcoholic fatty liver disease.* Hepatology, 2014. **59**(2): p. 471-82.
6. Mas, V.R., et al., *Genes involved in viral carcinogenesis and tumor initiation in hepatitis C virus-induced hepatocellular carcinoma.* Mol Med, 2009. **15**(3-4): p. 85-94.

Supplemental figure legends

Supplemental figure 1. FSTL1 expression in liver fibrosis tissues. (A-B) H&E staining, Masson's staining, and mRNA expression of TIMP-1 and COL1A1 in different histological stages of human liver fibrosis; **(C)** Proportion of $CD68^{+}FSTL1^{+}$ cells in $FSTL1^{+}$ cells in human liver fibrosis; **(D)** Analysis of FSTL1 expression in animal models of CCl_4 injection-, BDL- and MCD diet-induced fibrosis using three publicly available omics datasets. Human samples: Control (N=18), Mild fibrosis (N=20), Advanced fibrosis (N=13). Data were presented as mean ± SEM; **p < 0.01.

Supplemental figure 2. FSTL1 expression is primarily increased in macrophages in fibrotic liver tissues. (A) Double immunofluorescence staining of FSTL1 and α-SMA in human liver fibrosis. Scale bars, 50μm. (B) FSTL1 mRNA expression and (C) protein expression in isolated hepatocytes, HSCs and macrophages from mice liver fibrosis. Data were presented as mean ± SEM of at least three independent experiments; *p < 0.05, **p < 0.01.

Supplemental figure 3. There were no significant differences in the PKM2 mRNA levels in the FSTL1-knockout or FSTL1-overexpressing cells. Data were presented as mean ± SEM; N=6-8/group.

Supplemental figure 4. The expression of PKM2 was markedly increased in the nucleus of human liver fibrosis. N=6/group.

Supplemental figure 5. FSTL1-deficient BMDMs markedly reduced α-SMA expression and attenuated the activation of HSCs. (A) Cocultured HSCs with BMDMs in an LPS-induced inflammatory environment; **(B)** α-SMA expression was analyzed by WB; **(C)** α-SMA expression was analyzed by immunofluorescence staining. At least three independent experiments.

Supplemental figure 6. Generation and identification of myeloid-specific knockout mice. **(A)** Generation flow chart of myeloid-specific FSTL1 deficient mice; **(B)** Identification of myeloid-specific FSTL1 deficient mice.

Supplemental figure 7. Purity and viability of isolated macrophage were deducted. **(A)** Purity of isolated macrophage by the flowcytometry (F4/80 antibody); **(B)** Viability of isolated macrophage was examined after 0 or 24 h using a Countess II FL Automated Cell Counter with trypan blue exclusion.

Supplemental figure 8. All semi-quantitative analysis for the immunofluorescence staining in this study.

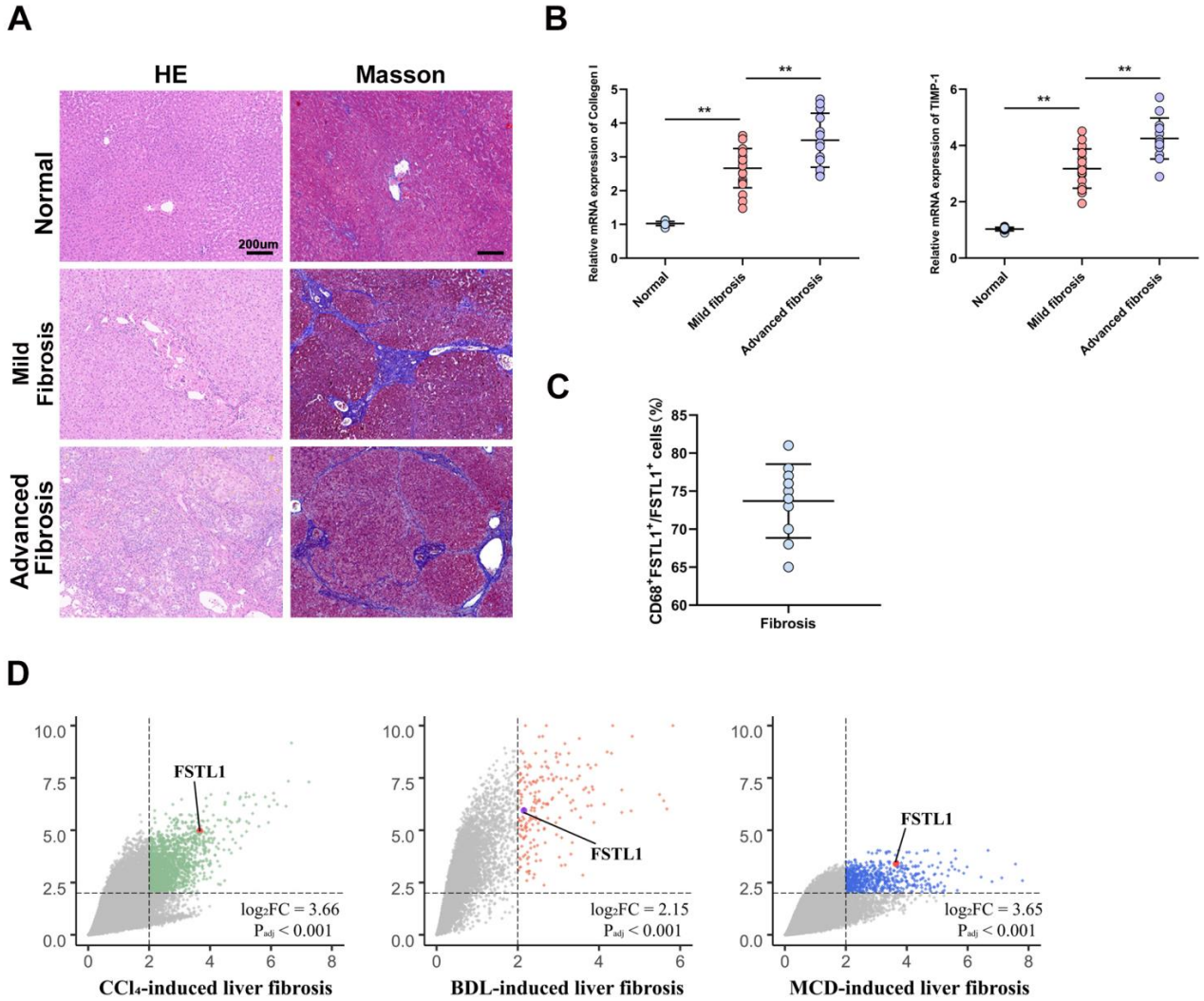

Supplemental Figure 1

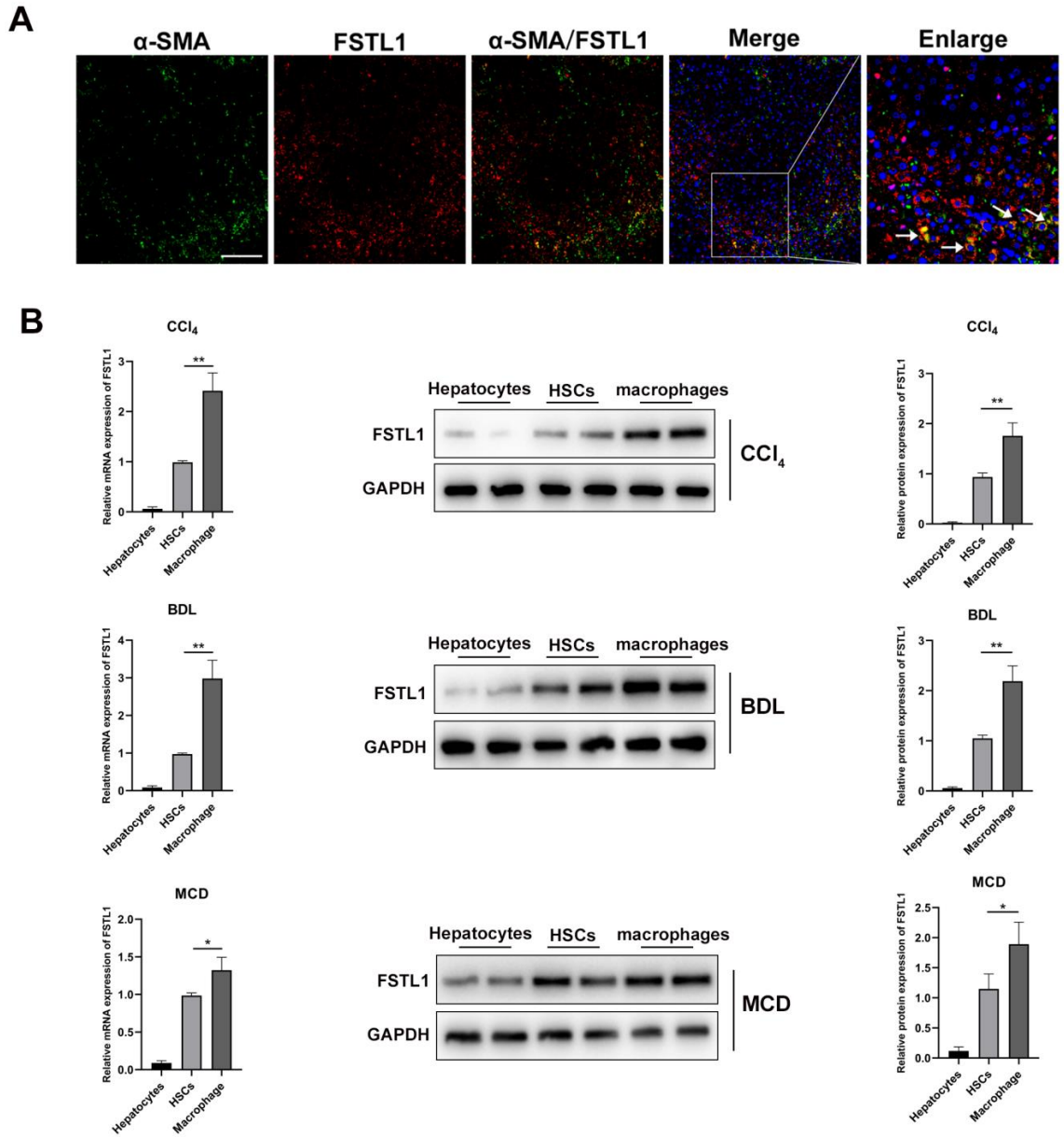

Supplemental Figure 2

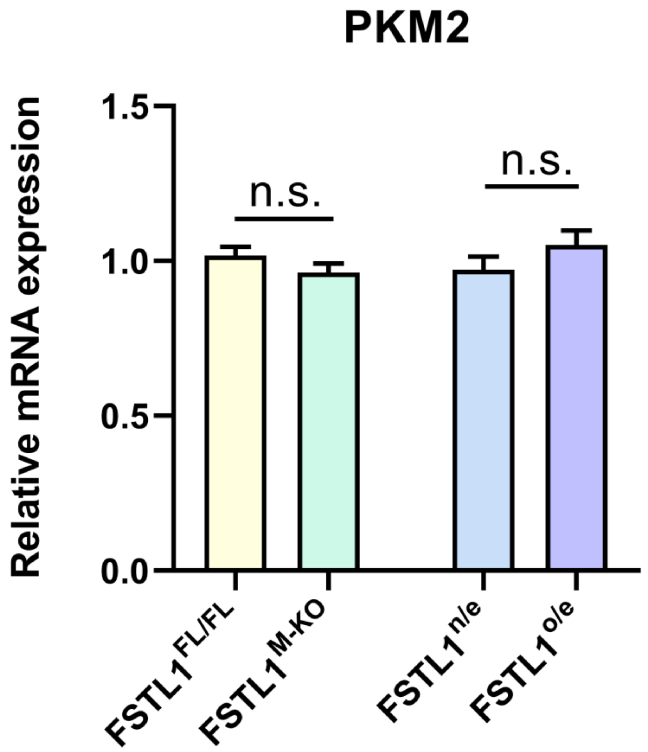

Supplemental Figure 3

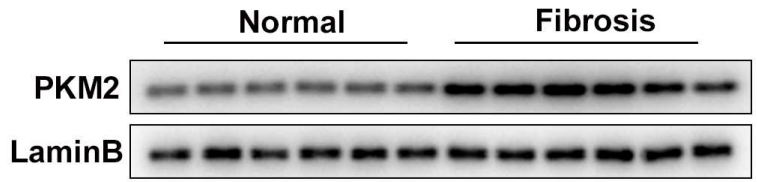

Supplemental Figure 4

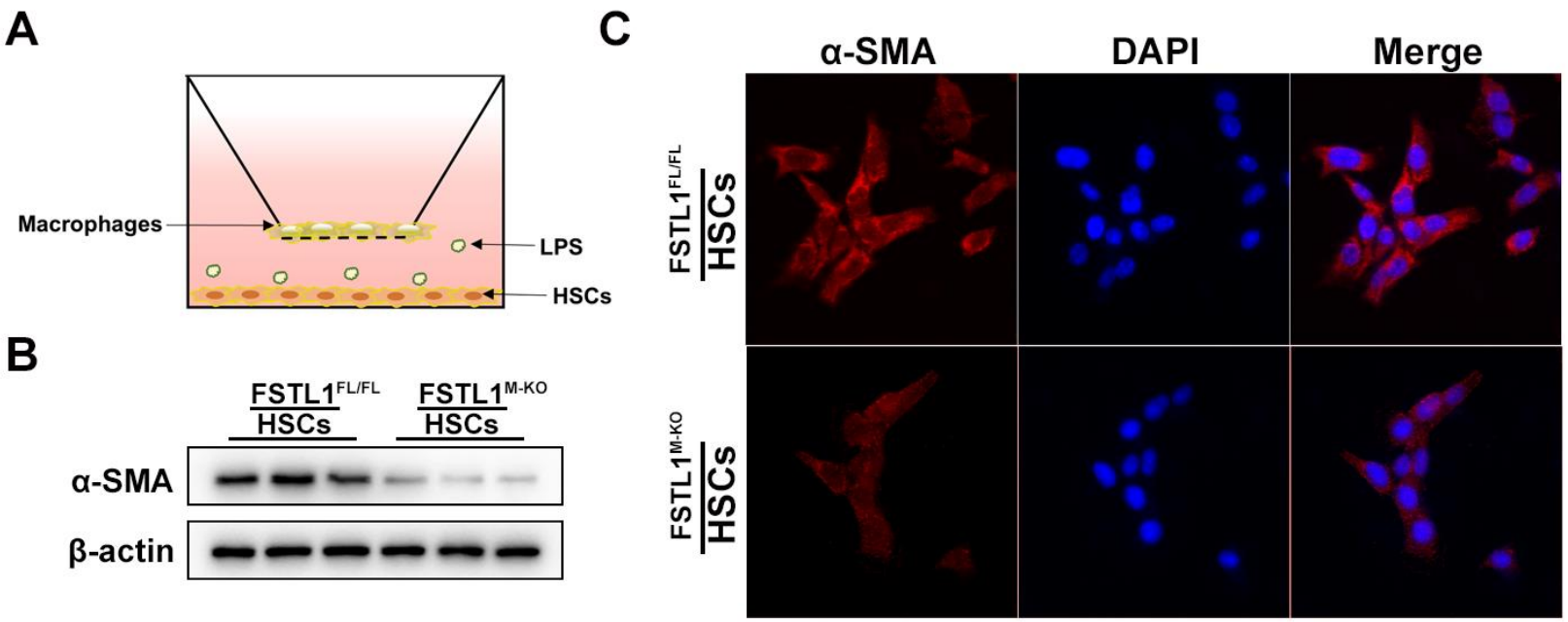

Supplemental Figure 5

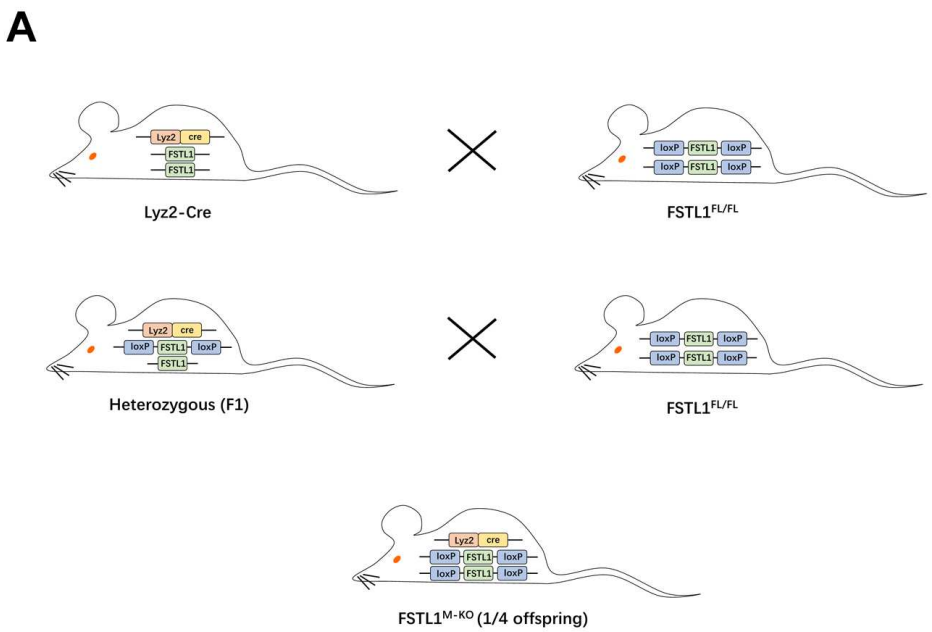

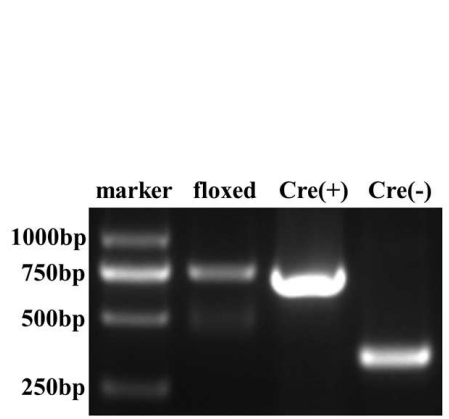

Supplemental Figure 6

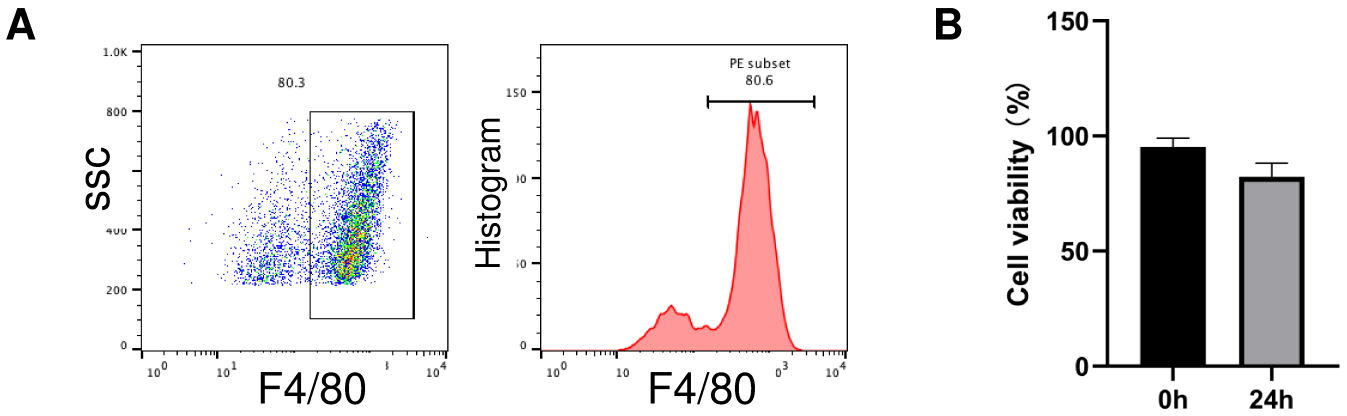

Supplemental Figure 7

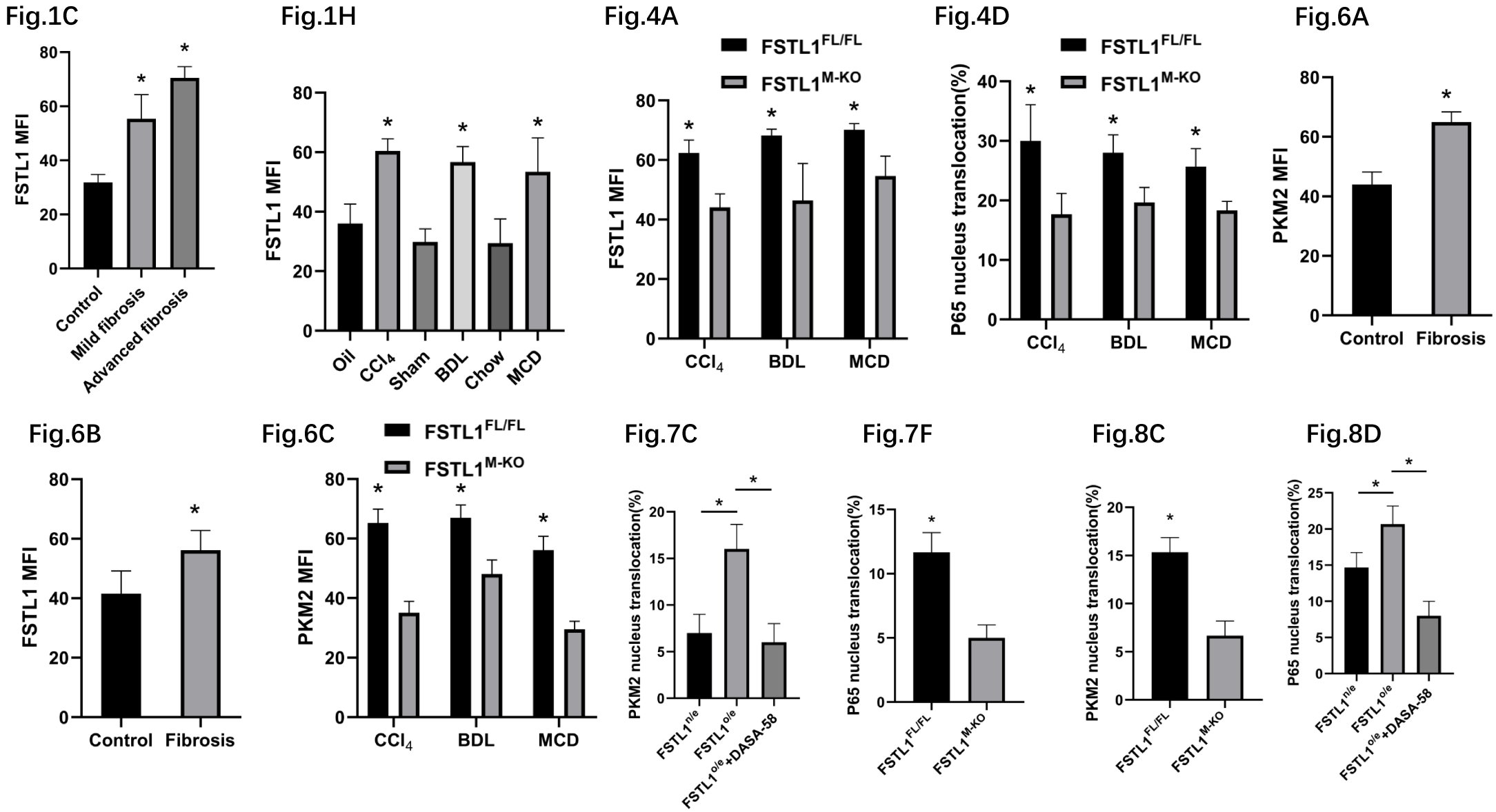

Supplemental Figure 8